Table 3
The number of training sets and test sets

(A)		
	Training	Test
Non HCC	43	11
HCC	41	13
(B)		
	Training	Test
Well	16	8
Moderate	20	7
(C)		
	Training	Test
AFP< 10(ng/ml)	20	4
AFP> 10(ng/ml)	14	10

(A) HCC, (B) histological grade, (C) AFP level.

a variable to class discrimination. Thus, we can eliminate irrelevant variables without any threshold. The R package used for stochastic gradient boosting, gbm, is available at http://cran.r-project.org.

3. Results and discussions

3.1. Proteomic profiling of non HCC and HCC tissues using 2D-DIGE

Labeled protein samples were separated on 2-DE, and fluorescence images were obtained. In parallel to the analytical gels, samples prepared from non HCC and HCC tissues were separately run on the preparative gels for protein identification. The proteins were visualized with SYPRO Ruby, and images were directly matched to CyDye images of analytical gels. Since 184 spots (125 proteins) consistently expressed in at least 70% of the all gels, we identified them as the proteins with consolidated expression intensities. Note that histological grade of moderate/well and high/low AFP level gels are derived from HCC samples only. Although we detected thousands spots on 2D gels, most of them are remained as unidentified. To enable us to interpret biologically, we analyzed identified spots only.

As mentioned in section 2.2, since the non HCC sample was labeled with Cy3 (or Cy5) dye, and the HCC sample was labeled with Cy5 (or Cy3) dye, we obtained three gels from one tissue sample. The numbers of HCC and non HCC gels, histological grade of moderate/well ones and high/low AFP ones are shown in Table 2.

3.2. Detection of proteins associated with HCC, histological grade and AFP level

To detect of the proteins associated with HCC, histological grade and AFP level, we performed supervised feature selection as described in section 2.10. To validate discriminative ability of selected spots, we randomly divided all gels to training sets and test sets. The number of training sets and test sets are summarized in Table 3. Since the number of HCC and non HCC gels was large, the rate of training sets and test sets was fixed about 4:1. On the other hand, since the number of images used to histological grade and AFP level was relatively small, the rate of training sets and test sets was set about 3:1 in cell differentiation and AFP level. We employed training sets for feature selection and constructing the predictive model. To detect spots associated with histological grade and AFP level, we used only HCC samples. The overall procedure is illustrated in Fig. 3. According to the previous study [21], we employed the parameters f, and M of SGB as 0.9, 0.01 and 1000, respectively. Table 4 show the selected spots associated with HCC, histological grade of moderate/well and AFP level. Other annotation data for these spots in Table S1 (Supplementary material). The number of selected spots associated with HCC, histological grade and AFP level is 18, 25 and 27, respectively. Although there are spots whose ratios are close to one, they are informative spots, because SGB is able to detect them as discriminative spots unlike statistical test for univariate, e.g., t-test. The positions of selected spots in the preparative 2D gel are shown in Fig. 4.

3.3. Evaluation of classification performance

We evaluated the classification performance by the selected spots on the basis of test sets according to the procedure illustrated in Fig. 3. This evaluation procedure is reasonable in terms of supervised prediction as discussed by Dupuy and Simon [27]. The performance was evaluated based on accuracy. Accuracy is defined as follows.

$$\text{accuracy} = \frac{\text{number of correctly predicted samples}}{\text{number of all samples}}$$

We constructed the predictive models using selected spots and training sets and applied to test sets as shown in Fig. 3. Table 5 shows the classification performance of SGB for HCC/non HCC, histological grade of moderate/well and high AFP (AFP>10(ng/ml))/low AFP (AFP< 10(ng/ml)) level. From Table 5, SGB is able to classify both training sets

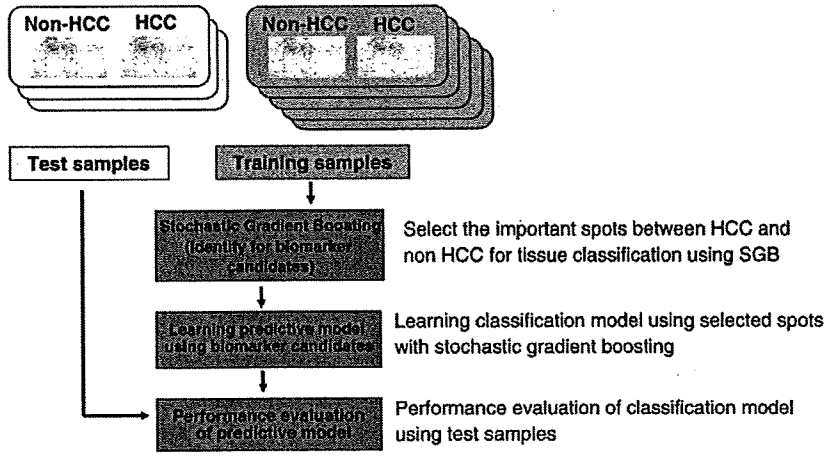

Fig. 3 Illustration of overall procedure for performance evaluation for HCC/non HCC classification. In histological grade of moderate/well grade and high/low AFP level, the same procedure is employed.

Table 4
Selected spots by SGB

(A) HCC

ID	SGB variable importance	Decyder		Protein name
		Ratio[a]	p-value (t-test)	
1977	30.66595	0.36	<1.0E−17	Carbonic anhydrase 2
560	29.66868	2.17	2.20E−13	Heat shock protein 90 kDa alpha
789	23.52533	1.84	2.20E−16	Annexin A6
1699	9.47421	6.98	<1.0E−17	Aldo-keto reductase family 1, member B10
366	3.07334	1.76	<1.0E−17	Heat shock 70 kDa protein 4
718	1.87712	2.12	5.70E−09	Heat shock 70 kDa protein 5
2012	0.71447	0.55	<1.0E−17	Enoyl Coenzyme A hydratase, short chain, 1
564	0.37075	1.37	0.0003	Transferrin
1007	0.15318	1.61	3.10E−07	Protein disulfide isomerase-associated 3
1556	0.12636	0.67	6.70E−10	Aldo-keto reductase 1A1
782	0.11134	1.7	1.40E−12	Heat shock 70 kDa protein 8
1331	0.05304	0.47	2.70E−13	Argininosuccinate synthetase
1312	0.05231	0.46	1.90E−09	Argininosuccinate synthetase
1046	0.05206	2.16	<1.0E−17	Vimentin
1582	0.04124	0.52	2.60E−11	Fructose-1,6-bisphosphatase 1
753	0.03851	1.79	3.60E−15	Heat shock 70 kDa protein 9B
2412	0.00211	0.54	3.00E−11	Human fatty acid binding protein FABP
444	0.00001	1.57	5.20E−06	Alpha glucosidase 2

(B) Histological grade

ID	SGB variable importance	Decyder		Protein name
		Ratio[b]	p-value (t-test)	
1129	49.9428	1.8	0.06	Keratin 8
1699	22.8444	0.43	2.00E−06	Aldo-keto reductase family 1, member B10
2423	5.616	1.38	0.064	D-dopachrome tautomerase
2126	4.7494	0.64	0.00041	peroxiredoxin 3
1068	4.6065	0.78	0.061	Glutamate dehydrogenase 1
2082	3.9313	0.77	0.0012	Es1 protein isoform 1a
1044	2.3596	0.61	0.068	Aldehyde dehydrogenase 1 family, member A1
999	1.6503	0.81	0.0033	Formiminotransferase cyclodeaminase
2039	1.2688	0.77	0.0088	Rho GDP dissociation inhibitor alpha
1685	1.1069	0.49	1.00E−05	Aldo-keto reductase 1B10
2025	0.6014	0.9	0.55	Heat shock 27 kDa protein 1
1036	0.4462	0.63	0.025	Aldehyde dehydrogenase 1 family, member A1
1059	0.3658	0.73	0.0054	Leucine aminopeptidase 3
1016	0.3094	0.98	0.11	Glucose regulated protein, 58 kDa
1027	0.0579	0.67	0.021	aldehyde dehydrogenase 1A1
1054	0.0558	0.73	0.015	Glutamate dehydrogenase 1
2159	0.0462	0.69	0.00038	Abhydrolase domain containing 14B
235	0.0204	1.13	0.48	Carbamoyl-phosphate synthetase 1
966	0.007	0.75	0.017	UDP-glucose dehydrogenase
2238	0.0044	0.93	0.054	Non-metastatic cells 1 protein
1086	0.003	0.98	0.87	UDP-glucose pyrophosphorylase 2
782	0.0025	1.19	0.25	Heat shock 70 kDa protein 8
2201	0.0018	0.76	0.025	Prostatic binding protein
1842	0.001	0.84	0.11	Electron-transfer-flavoprotein alpha subunit
798	0.0004	0.78	0.0021	Programmed cell death 8
1510	0.0004	0.78	0.0017	Acyl-Coenzyme A dehydrogenase, short/branched chain
1414	0.0001	0.93	0.14	Acetyl-Coenzyme A acetyltransferase 1

(C) AFP level

ID	SGB variable importance	Decyder		Protein name
		Ratio[c]	p-value (t-test)	
798	22.143	0.76	0.0002	Programmed cell death 8
1129	21.8696	1.62	0.25	Keratin 8
1007	12.4499	0.69	0.018	Protein disulfide isomerase-associated 3
1515	10.5222	0.81	0.95	Galactokinase 1
451	10.1806	0.85	0.37	Glucosidase, alpha; neutral AB
2159	7.1303	0.64	0.0065	Abhydrolase domain containing 14B
782	2.8347	1.18	0.0045	Annexin A6
659	2.7554	1.37	0.055	Lamin A/C
808	2.1413	0.7	0.0039	Carnitine palmitoyltransferase 2

Table 4 *(continued)*

(C) AFP level

ID	SGB variable importance	Decyder		Protein name
		Ratio[a]	p-value (t-test)	
1414	1.4418	0.81	0.01	Acetyl-Coenzyme A acetyltransferase 1
2082	1.4242	0.79	0.00028	Es1 protein isoform 1a
1219	1.2098	0.69	0.0083	Enolase 1
2010	1.1381	1.26	0.62	Enoyl-coenzyme A hydratase 1
1376	1.0921	0.61	0.00098	Actin, beta
2347	0.9536	1.35	0.001	Hemoglobin, beta
2364	0.2937	2.28	0.00013	Hemoglobin, beta
1794	0.1273	1.51	0.36	Sulfotransferase family, cytosolic, 2A, dehydroepiandrosterone-preferring, member 1
1383	0.0946	1.16	0.034	Aminoacylase 1
2423	0.0842	0.99	0.2	D-dopachrome tautomerase
1145	0.0647	0.95	0.058	ATP synthase, H+ transporting, mitochondrial F1 complex, beta polypeptide
1889	0.0281	1.12	0.41	Ketohexokinase
1795	0.0131	1.33	0.95	Sulfotransferase family, cytosolic, 2A, dehydroepiandrosterone (DHEA)-preferring, member 1
235	0.0045	0.87	0.063	Carbamoyl-phosphate synthetase 1, mitochondrial
1551	0.0028	1.35	0.7	Arginase 1
2039	0.0003	1.03	0.15	Rho GDP dissociation inhibitor alpha

[a] Ratio represents the average spot volume ratio of HCC/non HCC.
[b] Ratio represents the average spot volume ratio of moderate/well.
[c] Ratio represents the average spot volume ratio of high AFP/low AFP.

and test sets overall. For HCC and histological grade, SGB performs very well. For AFP, the accuracy of test sets is 71.4%. Although the performance of SGB depends on data sets, present results suggest that the spots selected by SGB are discriminative. From Table 4 (A)–(C), one can see that variable importance does not always correspond to *p*-value of *t*-test. This difference originates from that variable importance simultaneously incorporates multiple spots to classify the groups as described in Section 2.10, while *t*-test only incorporates average of each spots. Accordingly, one can detect the informative spots that contribute to sample classification through SGB. These discussions explain that SGB worked well for AFP in spite of the average spot value ratio of almost one.

To visualize the degree of discrimination for each data set by the selected spots, we show the scatter plots by two spots for each class in Fig. 5. One can see that the two spots discriminate each gel better than one spot. Thus, we demonstrated that supervised feature selection surely works well for detection of discriminative and informative proteins. Our results suggest that the SGB is able to detect the spots associated with tissue types using only identified spots.

3.4. Protein spots associated with HCC, histological grade and AFP

From Table 4(A), heat shock proteins (heat shock protein 90 kDa alpha, heat shock 70 kDa protein 4, heat shock 70 kDa protein 5, heat shock 70 kDa protein 8, heat shock 70 kDa protein 9B), protein disulfide isomerase-associated 3 (PDIA3) and aldo-keto reductase 1B10 (AKRB10) were overexpressed in HCC. These events are common at least three members of HSP family (HSP90, HSP70, HSC71) have been reported in prior works [14,28,29]. Members of the heat shock protein family have been known to promote cancer cell growth and survival by distinct mechanism [30]. HSP family were first discovered by their elevated abundance after heat shock. They take part in protein folding processes in normal physiological conditions. They bind and prevent non-native proteins from aggregation. Heat shock 70 kDa protein 5 (GRP78) is a member of HSP70 family localized in endoplasmic reticulum (ER). Expression of GRP78 can be induced in response to different stimuli including glucose starvation, hypoxia and ER

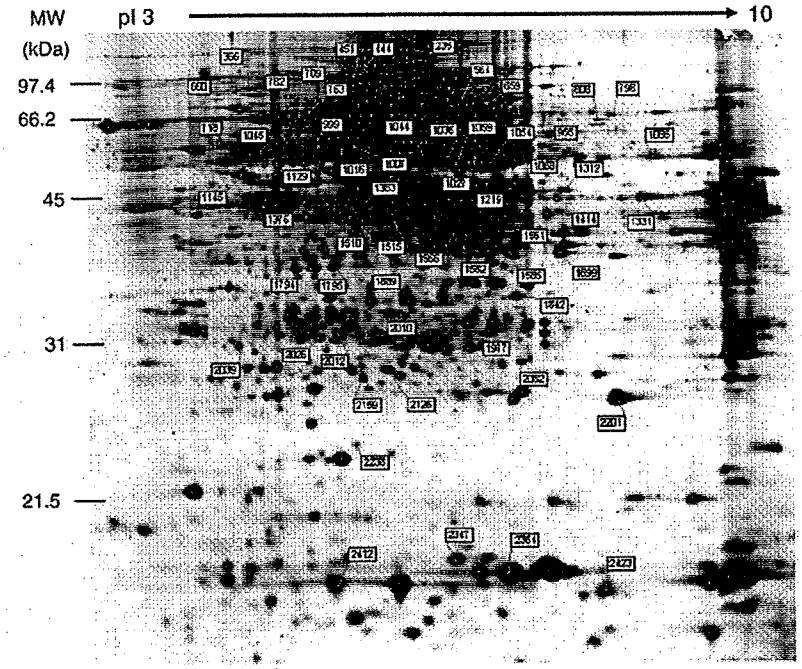

Fig. 4. Representative 2D image of the preparative gel. The gel was post-stained with SYPRO Ruby (Invitrogen). The numbers indicate spots associated with HCC, spots associated with grade and spots associated with AFP.

Ca2+ pool depletion [31]. GRP78 has been proven to protect cells from apoptosis, probably through inhibition of caspase-7 activation, an apoptotic executioner [32]. Highly induced GRP78 in progressively growing tumor cells has been reported to protect them from immune attack, thus preventing tumor regression [33]. High level of GRP78 observed in this study may also support the aggressive growth and the suppression of tumor rejection in HCC. In this study, carbonic anhydrase 2 (CAII) is poorly expressed in HCC, being consistent with the report of Kuo et al. [34] They concluded that this might promote tumor cell motility and contribute to tumor growth and metastasis.

In addition, heat shock 70 kDa protein 9B (mortalin) is abundantly expressed in HCC. Yi et al. [35] recently found that overexpression of mortalin in HCC was associated with HCC metastasis and early recurrence using 2-DE, quantitative PCR, western blot and immunohistochemistry. Poor expression of argininosuccinate synthetase (ASS) is one of well-known molecular features of HCC and is recently a target of HCC treatment using arginine-depleting enzymes [36]. Vimentin (VIM) is abundantly expressed in HCC. Hu et al. [37] reported that overexpression of VIM is significantly associated with HCC metastasis using cDNA microarray and tissue microarray.

Table 5
Performance evaluation for classification

Training sets	
Data sets	Accuracy (%)
HCC/non HCC	100
Moderate/well	100
Low AFP/high AFP	94.1
Test sets	
Data sets	Accuracy (%)
HCC/non HCC	100
Moderate/well	93.3
Low AFP/high AFP	71.4

(a) HCC (HCC/non HCC), (b) histological grade (moderate/well), (c) AFP level (low AFP/high AFP).

Furthermore, we examined gene expression level of selected proteins by RTD-PCR and cDNA microarray (Table S1 (a)). Most of these results are also consistent with protein expression profiles.

Although previous studies dealt with large size HCC or HCC with progressive stage, we dealt with small size HCC in this study. The proteins shown here might be potential biomarkers for early diagnosis.

Table 4 (B) and (C) represent protein spots associated with histological grade in HCC, and protein spots associated with AFP level, respectively. Table 4 (B) shows that several metabolic enzymes, such as AKRB10, glutamate dehydrogenase 1 (GLUD1), aldehyde dehydrogenase 1A1, and peroxiredoxin3 (PRDX3) were poorly expressed in moderate HCC cells, and keratin 8 (KRT8) were abundantly expressed in moderate HCC. It has been reported that the message of AKR1B10 was expressed most abundantly in small intestine and colon, while with lower levels in liver, thymus, prostate, testis, and skeletal muscle in normal tissues [38]. From our results, although AKR1B10 abundantly expressed in HCC compared with non HCC, it poorly expressed in moderate grade compared with well grade. The reason of this could be explained well, however different metabolic process in moderate differentiated HCC might not support the high expression of this gene as found in well differentiated HCC. GLUD1 has been reported poorly expressed in HCC [39]. This may suggest that GLUD1 is related to both HCC and grade. PRDX3 is required for MYC-mediated proliferation, transformation, and apoptosis after glucose withdrawal and essential for maintaining mitochondrial mass and membrane potential in transformed rat and human cells and deregulated expression of the MYC transcription factor is found in a wide variety of human tumors. These data provided evidence that PRDX3 is a MYC target gene that is required to maintain normal mitochondrial function [40].

AFP is the most established tumor marker in HCC and the gold standard by which other markers for the disease are judged [41]. Approximately, 70% of HCC are associated with AFP, and some HCC produce low level of AFP. Although small tumors tend to produce lower levels of AFP, direct relationship between serum AFP and tumor size has not been established as yet. Younger patients and men tend to have higher levels compared to older patients and women, respectively

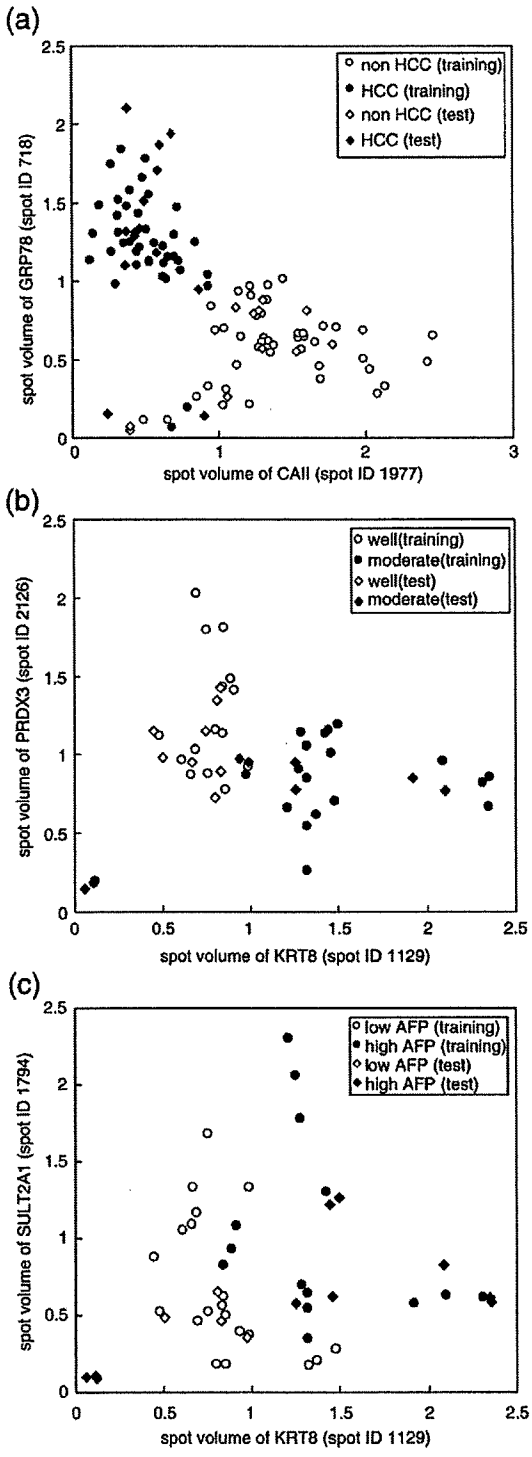

Fig. 5. The scatter plots by two spots. (a) HCC/non HCC, (b) histological grade of moderate/well, (c) high AFP/low AFP level.

[42,43]. From Table 4 (C), two structural protein, KRT8 and lamin A/C were abundantly expressed in HCC cells associated with higher levels of AFP, whereas two apotosis related proteins, programmed cell death 8 and sulfotransferase family, cytosolic, 2A, dehydroepiandrosterone-prefering, member1 (SULT2A1) and PDIA3 were poorly expressed in HCC cells associated with higher levels of AFP.

The overexpression of KRT8 also has been reported by Western blot and immunofluorescence analysis in higher metastatic HCC cell lines [44]. This implies that the alternation of KRT8 in its expression level might be related to metastatic ability. In this study, we observed that KRT8 expressed abundantly in both moderate HCC and high AFP level.

Chignard et al. has reported that a highly significant difference in PDIA3 fragment serum levels among HCC patients, at-risk patients (patients with chronic hepatitis or cirrhosis) and healthy individuals was observed [45]. However, they did not investigate the correlation between HCC and AFP. On the other hand, we observed that PDIA3 was poorly expressed in HCC cells associated with higher levels of AFP. Hence, our results suggest that AFP and PDIA3 may be complementarily expressed abundantly in serum.

Note that the differentially expressed proteins associated with histological grade of HCC and AFP level found in this study, are not always specific for HCC. PDIA3 has been reported to be differentially expressed in brain and breast cancer [46,47]. AKR1B10 has been involved also in lung cancer [48]. Also, it has been known that cytokeratins including KRT8 are part of the epithelial–mesenchymal transition (EMT). EMT is originally an embryonic developmental process that is hijacked by cancer cells in colorectal cancer [49]. However, our finding in this pilot study could provide new insights on understanding the pathogenesis of HCC, histological grade and AFP level.

4. Conclusion

We performed 2D-DIGE combined with MS to analyze the proteomic profiling of HCC and their surrounding non HCC obtained from 18 HCC patients. We identified the discriminative and informative protein spots associated with HCC, histological grade and AFP level using feature selection with SGB. We confirmed that the proposed method is able to identify known HCC-related proteins, e.g., HSP70 family. Moreover, we identified the potential biomarkers associated with histological grade of HCC and AFP level and found that AKR1B10 is related to,well differentiated HCC KRT8 is related to both cell differentiation and AFP level and PDIA3 is associated with both HCC and AFP level. Although the list of selected spots can be changed depending on training sets as pointed by Michiels et .al. [50], we showed that our present results for HCC are consistent with many prior studies and it appears that the obtained results are certainly reliable. Since all HCC samples were stage I, we observed the molecular events of relatively early stage of tumor. Our results shed light on understanding of the pathogenesis mechanism of HCC, histological grade and AFP level and will contribute to therapy and treatments for HCC. Although we only deal with small number of samples in this study, our strategy may be useful for detection of diagnosis or prognosis biomarkers when large number of samples are available.

Acknowledgement

The authors thank to Naoko Tetsura for excellent technical assistance.

Appendix A. Supplementary data

Supplementary data associated with this article can be found, in the online version, at doi:10.1016/j.bbapap.2008.02.011.

References

[1] D.M. Parkin, P. Pisani, J. Ferlay, Global cancer statistics, Cancer J. Clin. 49 (1999) 33–64.
[2] P. Pisani, D.M. Parkin, F. Bray, J. Ferley, Estimates of the world wide mortality from 25 cancers in 1990, Int. J. Cancer 83 (1999) 18–29.
[3] H.B. El-Serag, A.C. Mason, Rising incidence of hepatocelluar carcinoma in the United States, N. Engl. J. Med. 340 (1999) 745–750.

[4] S.D. Taylor-Robinson, G.R. Foster, S. Arora, H.C. Thomas, Increase in primary liver cancer in the UK, Lancet 350 (1997) 1142–1143.
[5] L.J. Lopez, J.A. Marrero, Hepatocellular carcinoma, Curr. Opin. Gastroenterol. 3 (2004) 248–253.
[6] H. Okabe, T. Satoh, T. Kato, O. Kitahara, R. Yanagawa, Y. Yamaoka, T. Tsunoda, Y. Furukawa, Y. Nakamura, Genomewide analysis of gene expression in human hepatocellular carcinomas using cDNA microarray: identification of genes involved in viral carcinogenesis and tumor progression, Cancer Res. 13 (2001) 2129–2137.
[7] X. Chen, S.T. Cheung, S. So, S.T. Fan, C. Barray, J. Higgins, K.M. Lai, J. Ji, S. Dudoit, I.O. Ng, M. Van De Rijn, D. Botstein, P.O. Brown, Gene expression patterns in human liver cancers, Mol. Biol. Cell 13 (2002) 1929–1939.
[8] M.W. Smith, Z.N. Yue, G.K. Geiss, N.Y. Sadovnikova, V.S. Carter, L. Boix, C.A. Lazaro, G.B. Rosenberg, R.E. Bumgarner, N. Fausto, J. Bruix, M.G. Katze, Identification of novel tumor markers in hepatitis C virus-associated hepatocellular carcinoma, Cancer Res. 63 (2003) 859–864.
[9] T. Yamashita, S. Kaneko, T. Hashimoto, S. Sato, N. Nagai, T. Toyoda, K. Suzuki, K. Kobayashi, K. Matsushima, Serial analysis of gene expression in chronic hepatitis C and hepatocellular carcinoma, Biochem. Biophys. Res. Commun. 282 (2001) 647–654.
[10] Q.H. Ye, L.X. Qin, M. Forgues, P. He, J.W. Kim, A.C. Peng, R. Simon, Y. Li, A.I. Robles, Y. Chen, Z.C. Ma, Z.Q. Wu, S. Ye, Y.K. Liu, Z.Y. Tang, X.W. Wang, Predicting hepatitis B virus-positive metastatic hepatocellular carcinoma using gene expression profiling and supervised machine learning, Nat. Med. 9 (2003) 416–423.
[11] P.J. Wirth, T.N. Hoang, T. Benjamin, Micorpreparative immobilized pH gradient two-dimensional electrophoresis in combination with protein microsequencing for the analysis of human liver proteins, Electrophoresis 16 (1995) 1946–1960.
[12] T.K. Seow, S.E. Ong, R.C. Liang, E.C. Ren, L. Chan, K. Ou, M.C. Chung, Two-dimensional electrophoresis map of the human hepatocellular carcinoma cell line, HCC-M, and identification of the separated proteins by mass spectrometry, Electrophoresis 21 (2000) 1787–1813.
[13] K.S. Park, S.Y. Cho, H. Kim, Y.K. Paik, Proteomic alternations of the variants of human aldehyde dehydrogenase isozymes correlate with hepatocellular carcinoma, Int. J. Cancer 97 (2002) 261–265.
[14] S.O. Lim, S.J. Park, W. Kim, S.G. Park, H.J. Kim, Y.I. Kim, T.S. Sohn, J.H. Noh, G. Jung, Proteomic analysis of hepatocellular carcinoma, Biochem. Biophys. Res. Commun. 291 (2002) 1031–1037.
[15] K.S. Park, H. Kim, N.G. Kim, S.Y. Cho, K.H. Choi, J.K. Seong, Y.K. Paik, Proteomic analysis and molecular characterization of tissue ferritin light chain in hepatocellular carcinoma, Hepatology 35 (2002) 1459–1466.
[16] M. Unlu, J.S. Morgan, J.S. Minden, Difference gel electrophoresis: a single gel method for detecting changes in protein extracts, Electrophoresis 11 (1997) 2071–2077.
[17] M.R. Knowles, S. Cervino, H.A. Skynner, S.P. Hunt, C. de Felipe, K. Salim, G. Meneses-Lorente, G. McAllister, P.C. Guest, Multiplex proteomic analysis by two-dimensional differential in gel electrophoresis, Proteomics 3 (2003) 1162–1171.
[18] J. Shaw, R. Rowlinson, J. Nickson, T. Stone, A. Sweet, K. Williams, R. Tonge, Evaluation of saturation labeling two-dimensional difference gel electrophoresis fluorescent dyes, Proteomics 3 (2003) 1181–1195.
[19] G. Van den Bergh, L. Arckens, Fluorescent two-dimensional difference gel electrophoresis unveils the potential of gel-based proteomics, Curr. Opin. Biotechnol. 15 (2004) 38–43.
[20] A. Alban, S.O. David, L. Bjorkesten, C. Anderson, E. Sloge, S. Lewis, I. Currie, A novel experimental design for comparative two-dimensional gel analysis: two-dimensional difference gel electrophoresis incorporating a pooled internal standard, Proteomics 1 (2003) 36–44.
[21] J.H. Friedman, Stochastic gradient boosting, Comput. Stat. Data Anal. 38 (2002) 367–378.
[22] K.G. Ishak, P.P. Anthony, L.H. Sobin, Histological typing Classification of Tumors, Springer-Verlag, New York, 1994.
[23] Minagawa, J., Honda, M., Miyazaki, K., Tabuse, Y., Teramoto, R., Yamashita, T., Nishino, K., Takatori, H., Ueda, T., Kamijo, K., Kaneko, S., Comparative proteomic and transcriptomic profiling of the human hepatocellular carcinoma. Biochem. Biophys. Res. Commun. in press.
[24] M. Honda, T. Yamashita, T. Ueda, R. Takatori, R. Nishino, S. Kaneko, Different signaling pathways in the livers of patients with chronic hepatitis B or chronic hepatitis C, Hepatology 44 (2006) 1122–1138.
[25] O. Troyanskaya, M. Cantor, G. Sherlock, P. Brown, T. Hastei, R. Tibshirani, D. Botstein, R.B. Altman, Missing value estimation methods for DNA microarrays, Bioinformatics 17 (2001) 520–525.
[26] J.H. Friedman, Greedy function approximation: a gradient boosting machine, Ann. Stat. 29 (2001) 1189–1232.
[27] A. Dupuy, R.M. Simon, Critical review of published microarray studies for cancer outcome and guidelines on statistical analysis and reporting, J. Natl. Cancer Inst. 99 (2007) 147–157 (99).
[28] M. Takashima, Y. Kuramitsu, Y. Yokoyama, N. Iizuka, T. Toda, I. Sakaida, K. Okita, M. Oka, K. Nakamura, Proteomic profiling of heat shock protein 70 family members as biomarkers for hepatitis C virus-related hepatocellular carcinoma, Proteomics 3 (2003) 2487–2493.
[29] W. Kim, S. Oe Lim, J.S. Kim, Y.H. Ryu, J.Y. Byeon, H.J. Kim, Y.I. Kim, J.S. Heo, Y.M. Park, G. Jung, Comparison of proteome between hepatitis B virus- and hepatitis C virus-associated hepatocelluar carcinoma, Clin. Cancer Res. 9 (2003) 5493–5500.
[30] M. Rohde, M. Daugaard, M.H. Jensen, K. Helin, J. Nylandsted, M. Jäättelä, Members of the heat-shock protein 70 family promote cancer cell growth by distinct mechanisms, Genes Dev. 19 (2005) 570–582.
[31] H. Miyake, I. Hara, S. Arakawa, S. Kamidono, Stress protein GRP78 prevents apoptosis induced by calcium ionophore, ionomycin, but not by glycosylation inhibitor, tunicamycin, in human prostate cancer cells, J. Cell. Biochem. 77 (2000) 396–408.
[32] R.K. Reddy, C. Mao, P. Baumeister, R.C. Austin, Endoplasmic reticulum chaperone protein GRP78 protects cells from apoptosis induced by topoisomerase inhibitors: role of ATP binding site in suppression of caspase-7 activation, J. Biol. Chem. 278 (2003) 20915–20924.
[33] C. Jamora, G. Dennert, A.S. Lee, Inhibition of tumor progression by suppression of stress protein GRP78/BiP induction in fibrosarcoma B/C10ME, Proc. Natl. Acad. Sci. U. S. A. 93 (1996) 7690–7694.
[34] W.H. Kuo, W.L. Chiang, S.F. Yang, K.T. Yeh, C.M. Yeh, Y.S. Hsieh, S.C. Chu, The differential expression of cytosolic carbonic anhydrase in human hepatocellular carcinoma, Life Sci. 73 (2003) 2211–2223.
[35] Yi, X., Luk, M. J., Lee, P. N., Peng, J., Leng, X., Guan, X., Lau, K. G., Fan, S., Association of mortalin (HSPA9) with liver cancer metastasis and prediction for early tumor recurrence. Mol. Cell. Proteomics. in press.
[36] N.P. Cheng, T. Lam, W. Lam, S. Tsui, W.A. Cheng, W. Lo, Y. Leung, Pegylated recombinant human arginase (rhArg-peg500mw) inhibits the in vitro and in vivo proliferation of human hepatocellular carcinoma through depletion, Cancer Res. 67 (2007) 309–317.
[37] L. Hu, H.S. Lau, C. Tzang, J. Wen, W. Wang, D. Xie, M. Huang, Y. Wang, M. Wu, J. Huang, W. Zeng, J. Sham, M. Yang, X. Guan, Association of vimentin overexpression and hepatocellular carcinoma metastasis, Oncogene 23 (2004) 298–302.
[38] D. Cao, S.T. Fans, S.S.M. Chung, Identification and characterization of a novel human aldose reductase-like gene, J. Biol. Chem. 273 (1998) 11429–11435.
[39] I.N. Lee, C.H. Chen, J.C. Sheu, H.S. Lee, G.T. Huang, C.Y. Yu, F.J. Lu, L.P. Chow, Identification of human hepatocellular carcinoma-related biomarkers by two-dimensional difference gel electrophoresis and mass spectrometry, J. Proteome Res. 4 (2005) 2062–2069.
[40] D.R. Wonsey, K.I. Zeller, C.V. Dang, The c-Myc target gene PRDX3 is required for mitochondrial homeostasis and neoplastic transformation, Proc. Natl. Acad. Sci. U. S. A. 99 (2002) 6649–6654.
[41] J.B. Lopez, Recent developments in the first detection of hepatocellular carcinoma, Clin. Biochem. Rev. 26 (2005) 65–79.
[42] M.C. Kew, Hepatocellular cancer: a century of progress, Clin. Liver Dis. 4 (2000) 257–268.
[43] P.J. Johnson, The role of serum alpha-fetoprotein estimation in the diagnosis and management of hepatocellular carcinoma, Clin. Liver Dis. 5 (2001) 145–160.
[44] Z. Dai, Y.K. Liu, J.F. Cui, H.L. Shen, J. Chen, R.X. Sun, Y. Zhang, X.W. Zhou, P.Y. Yang, Z.Y. Tang, Identification and analysis of altered alpha1,6-fucosylated glycoproteins associated with hepatocellular carcinoma metastasis, Proteomics 6 (2006) 5857–5867.
[45] N. Chignard, S. Shang, H. Wang, J. Marrero, C. Bréchot, S. Hanash, L. Bereretta, Cleavage of endoplasmic reticulum proteins in hepatocellular carcinoma: detection of generated fragments in patient sera, Gastroenterology 130 (2006) 2010–2022.
[46] F. Odreman, M. Vindigni, M.L. Gonzales, B. Niccolini, G. Candiano, B. Zanotti, M. Skrap, S. Pizzolitto, G. Stanta, A. Vindigni, Proteomic studies on low- and high-grade human brain astrocytomas, J. Proteome Res. 4 (2005) 698–708.
[47] K. Gumireddy, F. Sun, A.J. Klein-Szanto, J.M. Gibbins, P.A. Gimotty, A.J. Saunders, P.G. Schultz, Q. Huang, In vivo selection for metastasis promoting genes in the mouse, Proc. Natl. Acad. Sci. U. S. A. 16 (2007) 6696–6701.
[48] S. Fukumoto, N. Yamauchi, H. Moriguchi, Y. Hippo, A. Watanabe, J. Shibahara, H. Taniguchi, S. Ishikawa, H. Ito, S. Yamamoto, H. Iwanari, M. Hironaka, Y. Ishikawa, T. Niki, Y. Sohara, T. Kodama, M. Nishimura, M. Fukayama, H. Dosaka-Akita, H. Aburatani, Overexpression of the aldo-keto reductase family protein AKR1B10 is highly correlated with smokers' non-small cell lung carcinomas, Clin. Cancer Res. 5 (2005) 1776–1785.
[49] T. Knösel, V. Emde, K. Schlüns, P.M. Schlag, M. Dietel, I. Petersen, Cytokeratin profiles identify diagnostic signatures in colorectal cancer using multiplex analysis of tissue microarrays, Cell. Oncol. 28 (2006) 167–175.
[50] S. Michiels, S. Koscielny, C. Hill, Prediction of cancer outcome with microarrays: a multiple random validation strategy, Lancet 365 (2005) 488–492.

Available online at www.sciencedirect.com
ScienceDirect
Biochemical and Biophysical Research Communications 366 (2008) 186–192
BBRC
www.elsevier.com/locate/ybbrc

Comparative proteomic and transcriptomic profiling of the human hepatocellular carcinoma

Hirotaka Minagawa [a], Masao Honda [b,*], Kenji Miyazaki [c], Yo Tabuse [c,*], Reiji Teramoto [c], Taro Yamashita [b], Ryuhei Nishino [b], Hajime Takatori [b], Teruyuki Ueda [b], Ken'ichi Kamijo [a], Shuichi Kaneko [b]

[a] *Nano Electronics Research Laboratories, NEC Corporation, 34, Miyukigaoka, Tsukuba, Ibaraki 305-8501, Japan*
[b] *Department of Gastroenterology, Kanazawa University Graduate School of Medical Science, Kanazawa, 13-1 Takara-machi, Kanazawa 920-8641, Japan*
[c] *Bio-IT Center, NEC Corporation, 34, Miyukigaoka, Tsukuba, Ibaraki 305-8501, Japan*

Received 14 November 2007
Available online 4 December 2007

Abstract

Proteome analysis of human hepatocellular carcinoma (HCC) was done using two-dimensional difference gel electrophoresis. To gain an understanding of the molecular events accompanying HCC development, we compared the protein expression profiles of HCC and non-HCC tissue from 14 patients to the mRNA expression profiles of the same samples made from a cDNA microarray. A total of 125 proteins were identified, and the expression profiles of 93 proteins (149 spots) were compared to the mRNA expression profiles. The overall protein expression ratios correlated well with the mRNA ratios between HCC and non-HCC (Pearson's correlation coefficient: $r = 0.73$). Particularly, the HCC/non-HCC expression ratios of proteins involved in metabolic processes showed significant correlation to those of mRNA ($r = 0.9$). A considerable number of proteins were expressed as multiple spots. Among them, several proteins showed spot-to-spot differences in expression level and their expression ratios between HCC and non-HCC poorly correlated to mRNA ratios. Such multi-spotted proteins might arise as a consequence of post-translational modifications.

Keywords: Hepatocellular carcinoma; Proteome; Two-dimensional difference gel electrophoresis; Transcriptome; cDNA microarray

Hepatocellular carcinoma (HCC) is one of the most common cancers worldwide, and a leading cause of death in Africa and Asia [1]. Although several major risks related to HCC, such as hepatitis B and/or hepatitis C virus infection, aflatoxin B1 exposure, and alcohol consumption, and genetic defects, have been revealed [2], the molecular mechanisms leading to the initiation and progression of HCC are not well known. To find the molecular basis of hepatocarcinogenesis, comprehensive gene expression analyses have been done using many systems such as hepatoma cell lines and tissue samples [3,4]. Previously, we have carried out a comprehensive mRNA expression analysis using the serial analysis of gene expression (SAGE) [5] and cDNA microarray-based comparative genomic hybridization [6] to acquire the outline of gene expression profile of HCC. Although these genomic approaches have yielded global gene expression profiles in HCC and identified a number of candidate genes as biomarkers useful for cancer staging, prediction of prognosis, and treatment selection [7], the molecular events accompanying HCC development are not yet understood. In general, proteins rather than transcripts are the major effectors of cellular and tissue function [8] and it is accepted that protein expression do not always correlate with mRNA expression [9,10]. Thus, protein expression analysis, which could complement the available mRNA data, is also important to understand the molecular mechanisms of HCC.

* Corresponding authors. Fax: +81 76 234 4250 (M. Honda), +81 29 856 6136 (Y.Tabuse).
E-mail addresses: mhonda@medf.m.kanazawa-u.ac.jp (M. Honda), y-tabuse@cd.jp.nec.com (Y. Tabuse).

0006-291X/$ - see front matter © 2007 Elsevier Inc. All rights reserved.
doi:10.1016/j.bbrc.2007.11.101

The technique of two-dimensional difference gel electrophoresis (2D-DIGE), developed by Unlu et al. [11] is one of major advances in quantitative proteomics. Several groups have recently utilized 2D-DIGE to examine protein expression changes in HCC samples [12,13], whereas reports on the analysis combining both transcriptomic and proteomic approach are rare.

In the present study, we compared quantitatively protein expression profiles of HCC to non-HCC (non-cancerous liver) samples derived from 14 patients by 2D-DIGE. We also compared the protein expression profiles of the same HCC and non-HCC samples to the mRNA profiles which have been obtained using a cDNA microarray. The expression ratios of 93 proteins showed significant correlations with the mRNA ratios between HCC and non-HCC. Proteins involved in metabolic processes showed more prominent correlation. Our study describes an outline of gene and protein expression profiles in HCC, thus providing us a basis for better understanding of the disease.

Materials and methods

Patients. A total of 14 HCC patients who had surgical resection done in the Kanazawa University Hospital were enrolled. The clinicopathological characteristics of them are shown in Table 1. The HCC samples and adjacent non-tumor liver samples were snap frozen in liquid nitrogen, and used for cDNA microarray and 2D-DIGE analysis. All HCC and non-tumor samples were histologically diagnosed and quantitative detection of hepatitis C virus RNA by Amplicore analysis (Roche Diagnostic Systems) showed positive. The grading and staging of chronic hepatitis associated with non-tumor lesion were histologically assessed according to the method described by Desmet et al. [14] and histological typing of HCC was assessed according to Ishak et al. [15]. All strategies used for gene expression and protein expression analysis were approved by the Ethical Committee of Kanazawa University Hospital.

Preparation of cDNA microarray slides. In addition to in-house cDNA microarray slides consisting of 1080 cDNA clones as previously described [6,16–18], we made new cDNA microarray slides for detailed analysis of the signaling pathway of metabolism and enzyme function in liver disease [19]. Besides cDNA microarray analysis, a total of 256,550 tags were obtained from hepatic SAGE libraries (derived from normal liver, CH-C, CH-C related HCC, CH-B, and CH-B related HCC), including 52,149 unique tags. Among these, 16,916 tags expressing more than two hits were selected to avoid the effect of sequencing errors in the libraries. From these candidate genes, 9614 non-redundant clones were obtained from Incyte Genomics (Incyte Corporation), Clontech (Nippon Becton Dickinson), and Invitrogen (Invitrogen). Each clone was sequence validated and PCR amplified by Dragon Genomics (Takara Bio), and the cDNA microarray slides (Liver chip 10k) were constructed using SPBIO 2000 (Hitachi Software) as described previously [6,16–18].

Table 1
Characteristics of patients involved in this study

Patient No.	Age	Sex[a]	Histology of non-tumor lesion[b]	Tumor histology	Viral status
1	64	M	F4A1	Moderate	HCV
2	65	M	F4A1	Well	HCV
3	48	M	F3A1	Moderate	HCV
4	69	F	F4A2	Moderate	HCV
5	66	F	F4A2	Well	HCV
6	45	M	F4A1	Well	HCV
7	75	F	F4A1	Well	HCV
8	46	M	F4A2	Moderate	HCV
9	66	M	F2A2	Well	HCV
10	75	M	F3A1	Moderate	HCV
11	67	F	F4A2	Well	HCV
12	64	M	F4A1	Moderate	HCV
13	68	M	F4A0	Well	HCV
14	74	M	F1A0	Moderate	HCV

[a] M, male; F, female.
[b] F, fibrosis; A, activity.

RNA isolation and antisense RNA amplification. Total RNA was isolated from liver biopsy samples using an RNA extraction kit (Stratagene). Aliquots of total RNA (5 μg) were subjected to amplification with antisense RNA (aRNA) using a Message AmpTM aRNA kit (Ambion) as recommended by the manufacturer. About 25 μg of aRNA was amplified from 5 μg total RNA, assuming that 500-fold amplification of mRNA was obtained. The quality and degradation of the isolated RNA were estimated after electrophoresis using an Agilent 2001 bioanalyzer. In addition, 10 μg of aRNA was used for further labeling procedures.

Hybridization on cDNA microarray slides and image analysis. As a reference for each microarray analysis, aRNA samples prepared from the normal liver tissue from one of the patients were used. Test RNA samples fluorescently labeled with cyanine (Cy) 5 and reference RNA labeled with Cy3 were used for microarray hybridization as described previously [6,16–18]. Quantitative assessment of the signals on the slides was done by scanning on a ScanArray 5000 (General Scanning) followed by image analysis using GenePix Pro 4.1 (Axon Instruments) as described previously [6,16–18].

Protein expression analysis using 2D-DIGE. Protein samples were homogenized with lysis buffer (7 M urea, 2 M thiourea, 4% w/v CHAPS, 0.8 μM aprotinin, 15 μM pepstatin, 0.1 mM PMSF, 0.5 mM EDTA, 30 mM Tris–HCl, pH 8.5) and centrifuged at 13,000 rpm for 20 min at 4 °C. The supernatants were used as protein samples. The protein concentrations were determined with a protein assay reagent (Bio-Rad). The non-HCC and HCC samples (50 μg each) labeled with either Cy3 or Cy5 according to the manufacture's manual were combined and separated on 2-DE gels together with the Cy2-labeled internal standard (IS), which was prepared by mixing equal amounts of all samples. Analytical 2-DE was performed as described previously [20] using Immobiline DryStrip (pH 3–10, 24 cm, GE Healthcare) in the first dimension and 12.5% SDS–polyacrylamide gels (24 × 20 cm) in the second dimension. Samples were run in triplicate to obtain statistically reasonable results. After scanning with a Typhoon 9410 scanner (GE Healthcare), gels were silver stained for protein identification. For protein identification, 400 μg of the IS sample was also separately run on a 2-DE gel and stained with SYPRO Ruby (Invitrogen). All analytical and preparative gel images were processed using ImageQuant (GE Healthcare) and the protein level analysis was done with the DeCyder software (GE Healthcare). To detect phosphoproteins, 400 μg of HCC and non-HCC samples were separately run on 2-DE gels and stained with ProQ Diamond (Invitrogen). After acquiring images, gels were counterstained with SYPRO Ruby to visualize total proteins as described above.

Protein identification. The excised protein spots were in-gel digested with porcine trypsin (Promega). For LC-ESI-IT MS/MS analysis using LCQ Deca XP (Thermo Electron), the digested and dried peptides were dissolved in 10 μl of 0.1% formic acid in 2% acetonitrile (ACN). The dissolved samples were loaded onto C18 silica gel capillary columns (Magic C18, 50 × 0.2 mm), and the elution from the column was directly connected through a sprayer to an ESI-IT MS. Mobile phase A was 2% ACN containing 0.1% formic acid, and mobile phase B was 90% ACN containing 0.1% formic acid. A linear gradient from 5% to 65% of concentration B was applied to elute peptides. The ESI-IT MS was operated in positive ion mode over the range of 350–2000 (m/z) and the database search was carried out against the IPI Human using MASCOT (Matrixscience). The following search parameters were used: the cutting enzyme, trypsin; one missed cleavage allowed, mass tolerance window, ±1 Da, the MS/MS tolerance window, ±0.8 Da; carbamidomethyl cystein and oxidized methionine as fixed and variable modifications, respectively.

Detection of phosphorylated peptide. Possible phosphorylation sites were investigated by MALDI-TOF-MS using monoammonium phosphate (MAP) added matrix mainly according to Nabetani et al. [21]. An additive of MAP was mixed with α-CHCA matrix solution (5 mg/mL, 0.1% TFA, 50% ACN aqueous) to 40 mM in final concentration. Tryptsin digests of the spots positively stained with ProQ were dissolved into 4 μL of 0.1% TFA, 50% ACN aqueous solution and 1 μL of the peptides solution was spotted on the MALDI target plate. After drying up, 1 μL of the MAP matrix was dropped on the dried peptide mixture. Voyager DE-STR (ABI) was used to obtain mass spectra both in negative and positive ion mode. MS peaks that had relatively stronger intensities in negative ion mode than in positive ion mode were selected as candidates for acidically modified peptides.

Results and discussion

We identified 195 spots representing 125 proteins (Suppl. Table 1) and obtained the corresponding mRNA expression data for a total of 93 proteins (149 spots) (Suppl. Table 2). These 93 proteins were classified according to their biological processes and subcellular localizations into categories described by the Gene Ontology Consortium (http://www.geneontology.org/index.shtml) and about a half of them were related to metabolic processes (Fig. 1A). It is a general agreement that proteins with extremely high or low p*I* as well as hydrophobic proteins are difficult to be detected by 2-DE. Being consistent with this notion, our analysis detected many cytoplasmic proteins (Fig. 1B). Therefore, the protein expression data presented here were biased in favor of cytoplasmic and soluble proteins. The protein expression abundance between non-HCC and HCC was calculated using the normalized spot volume, which was the ratio of spot volume relative to IS (Cy3:Cy2 or Cy5:Cy2) and we used the Student's paired *t*-test ($p < 0.05$) to select the protein spots which were expressed differentially between non-HCC and HCC, using 2-DE gel images run in triplicate. The spot volume of a multi-spotted protein was indicated as a total volume by integrating the intensities of multiple spots as was done by Gygi et al. [10]. Comparison of protein expression profiles revealed that several proteins were expressed differentially between HCC and non-HCC. Proteins whose abundances increased >2-fold or decreased <1/2 in HCC are listed in Table 2. While glutamine synthetase, vimentin, annexin A2 and aldo-keto reductase were up-regulated, carbonic anhydrase 2, argininosuccinate synthetase 1, carbonic anhydrase 1, fructose-1,6-bisphosphatase 1, and betaine-homocysteine methyltransferase were down-regulated in HCC. Up- or down-regulation of most of these proteins in HCC has been reported previously [22–27]. Up-regulation of vimentin and annexin A2, and reduced expression of carbonic anhydrase 1 and 2 was suspected to be associated with cellular motility and metastasis [23,24,26].

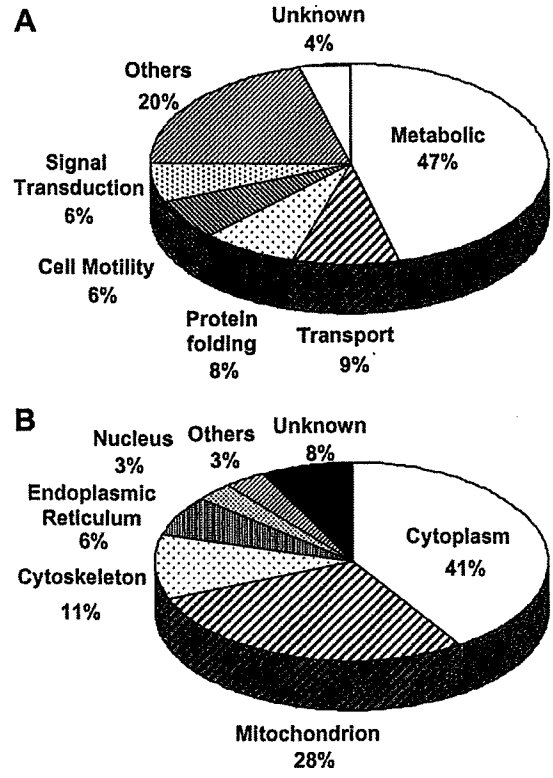

Fig. 1. Classification of identified proteins according to their cellular function (A) and subcellular localization (B).

The mRNA expression abundance was calculated from cDNA microarray data. Hierarchical clustering of

Table 2
Proteins expressed differentially between HCC and non-HCC

Spot ID	Protein name	Refseq ID	Theoretical		Fold change (HCC/non-HCC)		References
			p*I*	MW (kDa)	Protein[a]	mRNA	
1353, 1354	Glutamine synthase	NP_002056.2	6.43	42.7	2.06	3.08	[22]
1039, 1046	Vimentin	NP_003371	5.09	53.6	2.30	1.51	[23]
1716	Annexin A2	NP_001002857.1	7.57	38.8	2.57	1.82	[24]
1685, 1699	Aldo-keto reductase 1B10	NP_064695	7.12	36.2	4.29	4.73	[25]
1977	Carbonic anhydrase 2	NP_000058	6.87	29.3	0.39	0.62	[26]
1307, 1312, 1331	Argininosuccinate synthetase 1	NP_000041.2	8.08	46.8	0.41	0.30	[27]
1941	Carbonic anhydrase 1	NP_001729	6.59	28.9	0.47	1.25	[26]
1582	Fructose-1,6-bisphosphatase 1	NP_000498	6.54	37.2	0.48	0.36	
1256	Betaine-homocysteine methyltransferase	NP_001704	6.41	45.4	0.48	0.40	

[a] Integrated spot volume was used to calculate the fold change of multi-spotted proteins.

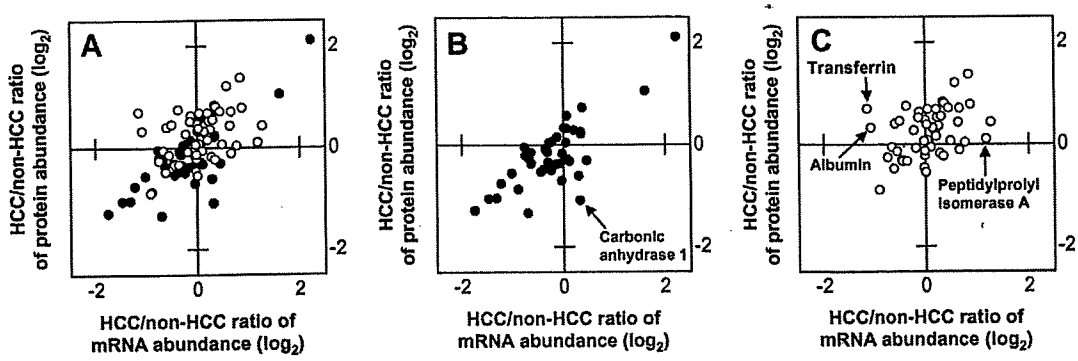

Fig. 2. Comparative analysis of protein and mRNA expression profiles between HCC and non-HCC. (A) The HCC/non-HCC ratios of averaged protein expression levels for 93 proteins were plotted against those of mRNA. Proteins related to metabolic pathways were indicated in closed circles and were shown again in (B). Proteins related to the other biochemical pathways were indicated in open circles and shown in (C). Proteins listed in Table 3 were indicated in (B) and (C). All graphs were depicted in $\log_2$ scale.

Table 3
Proteins whose expression changes between HCC and non-HCC show poor correlation to mRNA expression changes

Spot ID	Protein name	Refseq ID	Theoretical		Spot[a] Av. Ratio	Spot *p* value	Protein ratio	Micro array Av. ratio	Micro array *p* value
			*p*I	MW (kDa)					
564	Transferrin	NP_001054	6.8	79.3	2.23	0.035	1.61	0.45	3.3E−06
565					1.87	0.079			
566					2.28	0.13			
605					0.73	0.098			
1489	Albumin	NP_000468	5.9	71.3	—	0.63	1.25	0.47	2.3E−03
1941	Carbonic anhydrase 1	NP_001729	6.6	28.9	—	3.5E−03	0.47	1.25	0.39
2290	Peptidylprolyl isomerase A	NP_066953	7.7	18.1	—	5.0E−01	1.07	2.29	1.1E−01

[a] Since transferrin was detected in multiple spots, averaged ratio and spot *p* value of each spot is shown.

Table 4
Multi-spotted proteins showing spot-to-spot differences in expression level between non-HCC and HCC

Spot ID	Spot Av. ratio	Spot *p* value	Protein name	Refseq ID	Theoretical		Protein[a] ratio
					*p*I	MW (kDa)	
436	1.92	5.3E−04	Tumor rejection antigen (gp96)	NP_003290	4.8	92.7	1.2
537	0.79	0.16					
564	2.23	0.035	Transferrin	NP_001054	6.8	79.3	1.61
565	1.87	0.079					
566	2.28	0.13					
605	0.73	0.098					
1257	1.02	0.92	Fumarate hydratase	NP_000134	8.8	54.8	0.8
1261	0.6	1.3E−03					

[a] HCC/non-HCC protein ratios were calculated using integrated spot abundances.

gene expression was done with BRB-ArrayTools (http://linus.nci.nih.gov/BRB-ArrayTools.htm). The filtered data were log-transferred, normalized, centered, and applied to the average linkage clustering with centered correlation. BRB-ArrayTools contains a class comparison tool based on univariate *F* tests to find genes differentially expressed between predefined clinical groups. The permutation distribution of the *F* statistic, based on 2000 random permutations, was also used to confirm statistical significance. A *p* value of less than 0.05 for differences in HCC/non-HCC gene expression ratio was considered significant.

The average HCC/non-HCC expression ratios of the 93 proteins were plotted against the mRNA ratios in Fig. 2, where a positive value indicates increased expression in HCC and a negative ratio indicates reduced expression. The overall expression ratio of HCC/non-HCC indicated noticeable correlation between protein and mRNA

(Fig. 2A), and the Pearson's correlation coefficient for this data set (93 proteins/genes) was 0.73. Next, we divided 93 proteins into those related to metabolism and others biological processes. The HCC/non-HCC ratios of protein expression for metabolism-related proteins showed substantial correlation with those of mRNA (Fig. 2B, $r = 0.9$), whereas those of other proteins were poorly correlated (Fig. 2C, $r = 0.36$). Extreme care must be taken in a direct comparison of proteomic data with transcriptome because of multiple layers of discrepancies caused by the distinct sensitivities of cDNA array hybridization and 2-DE, the inability of a cDNA array to distinguish mRNA isoforms and post-translational modifications of proteins. Nevertheless, our results suggest that the expression of considerable portion of proteins with metabolic function listed here is regulated at transcriptional level. On the other hand, post-transcriptional and/or post-translational processes seem to be involved in the regulation of expression level for proteins with other cellular functions as a whole. Four proteins (albumin, transferrin, peptidylproryl isomerase A, and carbonic anhydrase 1) showed apparent poor correlation in protein and mRNA expression profiles (Table 3 and Fig. 2). Transcriptional control might have little effect on the expression changes of these proteins between HCC and non-HCC.

A number of proteins were expressed as multiple spots on 2-DE gels and most multi-spotted proteins showed little spot-to-spot variations in the averaged HCC/non-HCC ratio. Although we do not know how these multiple spots were generated, many of them might be due to the conformational equilibrium of proteins under electrophoresis rather than to any post-translational modifications [28]. On the other hand, the HCC/non-HCC expression ratios of several multi-spotted proteins varied from spot to spot, and three proteins (transferrin, fumarate hydratase, and tumor rejection antigen gp96) were categorized as these multi-spotted proteins (Table 4).

For example, gp96 was detected in two spots (spot #436 and 537) with distinct molecular mass and p*I* and they showed different HCC/non-HCC expression ratio (Fig. 3A and B and Table 4). The expression of these two isoforms was observed to change in the opposite direction between non-HCC and HCC: #436 was up-regulated in HCC (HCC/non-HCC ratio: 1.96) while #537 was down-regulated (HCC/non-HCC ratio: 0.79) (Table 4 and Fig. 3C and D). Gp96 is a glycoprotein present in endoplasmic reticulum and is supposed to function as a molec-

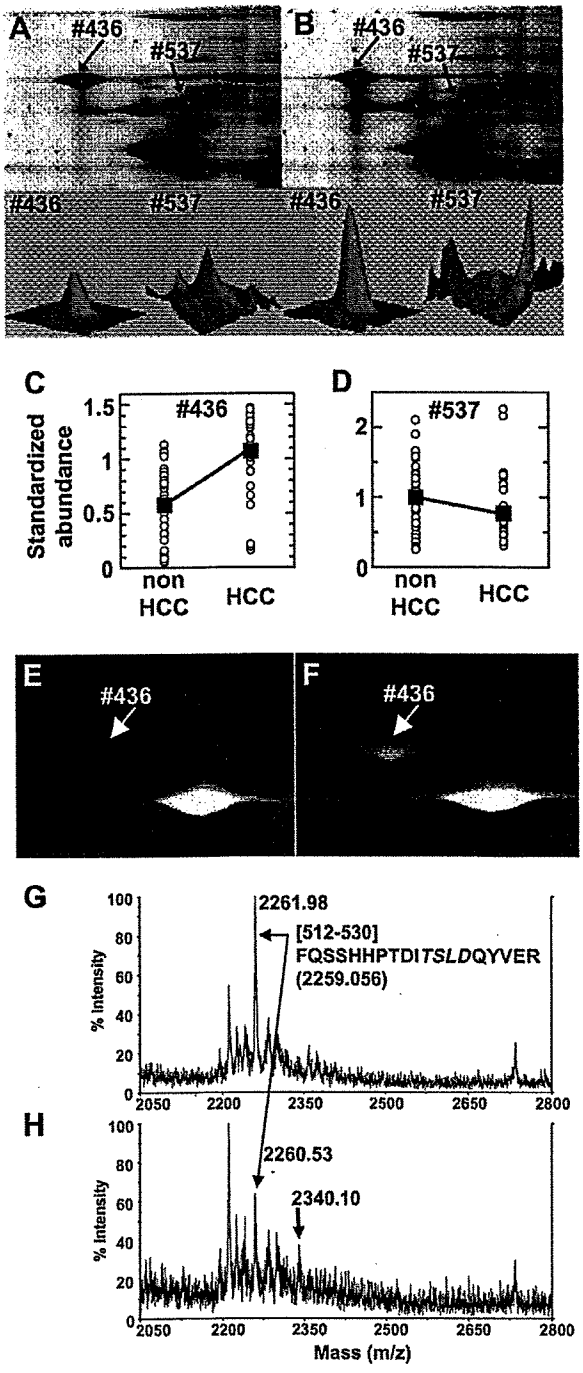

Fig. 3. Comparison of expression profiles of two gp96 spots between HCC and non-HCC. The expression profile and phosphorylation of tumor rejection antigen gp96 in HCC and non-HCC was investigated. Magnified gel images and 3D views of two gp96 spots in non-HCC (A) and HCC (B) were shown. Differences in expression level of two gp96 spots, #436 (C) and #537 (D), between non-HCC and HCC were shown. The open circle indicates the standardized abundance of the individual spot in each sample. The closed square represents the averaged abundance of each gp96 spot. Magnified gel images of non-HCC (E) and HCC (F) stained with ProQ. The #436 spot was positively stained with ProQ, while unambiguous staining of the #537 spot was not observed. Tryptic peptides prepared from the spot #436 were analyzed by MALDI–TOF mass-spectrometry in the positive ion mode (G) and the negative ion mode (H). A peak of 2261.98 detected in positive ion mode corresponds to the amino acid sequence from 512 to 530. In addition to the original peak (*m/z*: 2260.53), a peak mass shifted by +80 Da was detected in the negative ion mode. A predicted phosphorylation consensus motif for protein kinase CK2 is indicated in italics (G).

ular chaperone and intracellular Ca^{2+} regulator [29,30]. Several previous reports have shown that gp96 is glycosylated and phosphorylated, and exists as heterogeneous molecular entities with various molecular weights [31]. In order to know whether gp96 spots were phosphorylated or not, we stained the 2-DE gels with ProQ Diamond which is a dye specific to proteins phosphorylated on serine, threonine or tyrosine residues [32], and has been used successfully to visualize phosphoproteins [33]. We found that the spot #436 was positively stained with ProQ (Fig. 3E and F). We further tried to detect possible phosphorylated peptides in the tryptic digests prepared from #436 by MALDI–TOF–MS according to Nabetani et al. [21]. Searching for those peaks that had relatively stronger intensities in negative ion mode than in positive ion mode, we found two peaks as candidates for acidically modified peptides. They were assigned to the peptides SILFVPTSAPR (amino acid sequence: 385–395, data not shown) and FQSSHHPTDITSLDQYVER (aa512–530). Fig. 3G and H show the unmodified peak and the acidically modified peak (mass shifted by +80 Da in negative ion mode) of the latter peptide, respectively. This peptide contained a predicted phosphorylation consensus motif, [Ser or Thr]-X-X-[Asp or Glu], for protein kinase CK2 (Fig. 3G) which was suggested to phosphorylate gp96 [34]. These results together with ProQ staining indicated that at least one gp96 isoform was phosphorylated and was up-regulated in HCC. Over-expression of gp96 in HCC has been reported previously [35], though the reports that showed over-expression of its phosphorylated form are rare. Further investigation into biological meaning of gp96 phosphorylation may provide us important information about HCC development.

Acknowledgments

We thank the late Dr. A. Tsugita for helpful discussion through this work and N. Tetsura for technical assistance.

Appendix A. Supplementary data

Supplementary data associated with this article can be found, in the online version, at doi:10.1016/j.bbrc.2007.11.101.

References

[1] T.K. Seow, R.C.M.Y. Liang, C.K. Leow, M.C.M. Chung, Hepatocellular carcinoma: from bedside to proteomics, Proteomics 1 (2001) 1249–1263.
[2] L.J. Lopez, J.A. Marrero, Hepatocellular carcinoma, Curr. Opin. Gastroenterol. 3 (2004) 248–253.
[3] H.F. Kawai, S. Kaneko, M. Honda, Y. Shirota, K. Kobayashi, Alpha-fetoprotein-producing hepatoma cell lines share common expression profiles of genes in various categories demonstrated by cDNA microarray analysis, Hepatology 3 (2001) 676–691.
[4] N. Iizuka, M. Oka, H. Yamada-Okabe, N. Mori, T. Tamesa, T. Okada, N. Takemoto, K. Hashimoto, et al., Differential gene expression in distinct virologic types of hepatocellular carcinoma: association with liver cirrhosis, Oncogene 22 (2003) 3007–3014.
[5] T. Yamashita, S. Kaneko, S. Hashimoto, T. Sato, S. Nagai, N. Toyoda, T. Suzuki, K. Kobayashi, et al., Serial analysis of gene expression in chronic hepatitis C and hepatocellular carcinoma, Biochem. Biophys. Res. Commun. 282 (2001) 647–654.
[6] K. Kawaguchi, M. Honda, T. Yamashita, Y. Shirota, S. Kaneko, Differential gene alteration among hepatoma cell lines demonstrated by cDNA microarray-based comparative genomic hybridization, Biochem. Biophys. Res. Commun. 329 (2005) 370–380.
[7] Y. Midorikawa, M. Makuuchi, W. Tang, H. Aburatani, Microarray-based analysis for hepatocellular carcinoma: from gene expression profiling to new challenges, World J. Gastroenterol. 13 (2007) 1487–1492.
[8] N.A. Shackel, D. Seth, P.S. Haber, M.D. Gorrell, G.W. McCaughan, The hepatic transcriptome in human liver disease, Comp. Hepatol. 5 (6) (2006).
[9] T.J. Griffin, S.P. Gygi, T. Ideker, B. Rist, J. Eng, L. Hood, R. Aebersold, Complementary profiling of gene expression at the transcriptome and proteome levels in *Saccharomyces cerevisiae*, Mol. Cell. Proteomics 4 (2002) 323–333.
[10] S.P. Gygi, Y. Rochon, B.R. Franza, R. Aebersold, Correlation between protein and mRNA abundance in yeast, Mol. Cell. Biol. 19 (1999) 1720–1730.
[11] M. Unlu, M.E. Morgan, J.S. Minden, Difference gel electrophoresis: a single gel method for detecting changes in protein extracts, Electrophoresis 11 (1997) 2071–2077.
[12] I.N. Lee, C.H. Chen, J.C. Sheu, H.S. Lee, G.T. Huang, C.Y. Yu, F.J. Lu, L.P. Chow, Identification of human hepatocellular carcinoma-related biomarkers by two-dimensional difference gel electrophoresis and mass spectrometry, J. Proteome Res. 6 (2005) 2062–2069.
[13] C.R. Liang, C.K. Leow, J.C. Neo, G.S. Tan, S.L. Lo, J.W. Lim, T.K. Seow, P.B. Lai, et al., Proteome analysis of human hepatocellular carcinoma tissues by two-dimensional difference gel electrophoresis and mass spectrometry, Proteomics 5 (2005) 2258–2271.
[14] V.J. Desmet, M. Gerber, J.H. Hoofnagle, M. Manns, P.J. Scheuer, Classification of chronic hepatitis: diagnosis, grading and staging, Hepatology 19 (1994) 1513–1520.
[15] K.G. Ishak, P.P. Anthony, L.H. Sobin, Histological typing of tumours of the liver, 2nd ed.WHO International Histological Classification of Tumors, Springer-Verlag, New York, 1994.
[16] M. Honda, S. Kaneko, H. Kawai, Y. Shirota, K. Kobayashi, Differential gene expression between chronic hepatitis B and C hepatic lesion, Gastroenterology 120 (2001) 955–966.
[17] H.F. Kawai, S. Kaneko, M. Honda, Y. Shirota, K. Kobayashi, Alpha-fetoprotein-producing hepatoma cell lines share common expression profiles of genes in various categories demonstrated by cDNA microarray analysis, Hepatology 33 (2001) 676–691.
[18] M. Honda, H. Kawai, Y. Shirota, T. Yamashita, T. Takamura, S. Kaneko, cDNA microarray analysis of autoimmune hepatitis, primary biliary cirrhosis and consecutive disease manifestation, J. Autoimmun. 25 (2005) 133–140.
[19] M. Honda, T. Yamashita, T. Ueda, H. Takatori, R. Nishino, S. Kaneko, Different signaling pathways in the livers of patients with chronic hepatitis B or chronic hepatitis C, Hepatology 44 (2006) 1122–1138.
[20] Y. Tabuse, T. Nabetani, A. Tsugita, Proteomic analysis of protein expression profiles during *Caenorhabditis elegans* development using 2D-difference gel electrophores, Proteomics 5 (2005) 2876–2891.
[21] T. Nabetani, K. Miyazaki, Y. Tabuse, A. Tsugita, Analysis of acidic peptides with a matrix-assisted laser desorption/ionization mass spectrometry using positive and negative ion modes with additive monoammonium phosphate, Proteomics 6 (2006) 4456–4465.
[22] Y. Kuramitsu, T. Harada, M. Takashima, Y. Yokoyama, I. Hidaka, N. Iizuka, T. Toda, M. Fujimoto, et al., Increased expression and phosphorylation of liver glutamine synthetase in well-differentiated

hepatocellular carcinoma tissues from patients infected with hepatitis C virus, Electrophoresis 27 (2006) 1651–1658.
[23] L. Hu, S.H. Lau, C.H. Tzang, J.M. Wen, W. Wang, D. Xie, M. Huang, Y. Wang, et al., Association of Vimentin overexpression and hepatocellular carcinoma metastasis, Oncogene 23 (2004) 298–302.
[24] Z. Dai, Y.K. Liu, J.F. Cui, H.L. Shen, J. Chen, R.X. Sun, Y. Zhang, X.W. Zhou, Identification and analysis of altered alpha1,6-fucosylated glycoproteins associated with hepatocellular carcinoma metastasis, Proteomics 6 (2006) 5857–5867.
[25] E. Zeindl-Eberhart, S. Haraida, S. Liebmann, P.R. Jungblut, S. Lamer, D. Mayer, G. Jäger, S. Chung, H.M. Rabes, Detection and identification of tumor-associated protein variants in human hepatocellular carcinomas, Hepatology 39 (2004) 540–549.
[26] W.H. Kuo, W.L. Chiang, S.F. Yang, K.T. Yeh, C.M. Yeh, Y.S. Hsieh, S.C. Chu, The differential expression of cytosolic carbonic anhydrase in human hepatocellular carcinoma, Life Sci. 73 (2003) 2211–2223.
[27] P.N. Cheng, T.L. Lam, W.M. Lam, S.M. Tsui, A.W. Cheng, W.H. Lo, Y.C. Leung, Pegylated recombinant human arginase (rhArgpeg5,000mw) inhibits the in vitro and in vivo proliferation of human hepatocellular carcinoma through arginine depletion, Cancer Res. 67 (2007) 309–317.
[28] F.S. Berven, O.A. Karisen, J.C. Murrell, H.B. Jensen, Multiple polypeptide forms observed in two-dimensional gels of Methylococcus capsulatus (Bath) polypeptides are generated during the separation procedure, Electrophoresis 24 (2003) 757–761.
[29] J. Melnick, S. Aviel, Y. Argon, The endoplasmic reticulum stress protein GRP94, in addition to BiP, associates with unassembled immunoglobulin chains, J. Biol. Chem. 267 (1992) 21303–21306.
[30] H. Liu, E. Miller, B. van de Water, J.L. Stevens, Endoplasmic reticulum stress proteins block oxidant-induced Ca^{2+} increases and cell death, J. Biol. Chem. 273 (1998) 12858–12862.
[31] A.M. Feldweg, P.K. Srivastava, Molecular heterogeneity of tumor rejection antigen/heat shock protein GP96, Int. J. Cancer 63 (1995) 310–314.
[32] T.H. Steinberg, B.J. Agnew, K.R. Gee, W.-Y. Leung, T. Goodman, B. Schulenberg, J. Hendrickson, J.M. Beechem, R.P. Haugland, W.F. Patton, Global quantitative phosphoprotein analysis using multiplexed proteomics technology, Proteomics 3 (2003) 1128–1144.
[33] B.R. Chitteti, Z. Peng, Proteome and phosphoproteome dynamic change during cell dedifferentiation in Arabidopsis, Proteomics 7 (2007) 1473–1500.
[34] S.E. Cala, GRP94 hyperglycosylation and phosphorylation in Sf21 cells, Biochim. Biophys. Acta 1496 (2000) 296–310.
[35] D.F. Yao, X.H. Wu, X.Q. Su, M. Yao, W. Wu, L.W. Qiu, L. Zou, X.Y. Meng, Abnormal expression of HSP gp96 associated with HBV replication in human hepatocellular carcinoma, Hepatobiliary Pancreat. Dis. Int. 5 (2006) 381–386.

Hepatitis B virus X protein overcomes oncogenic RAS-induced senescence in human immortalized cells

Naoki Oishi,[1,2] Khurts Shilagardi,[1] Yasunari Nakamoto,[2] Masao Honda,[2] Shuichi Kaneko[2] and Seishi Murakami[1,3]

[1]Department of Signal Transduction, Cancer Research Institute; [2]Department of Disease Control and Homeostasis, Graduate School of Medicine, Kanazawa University, 13-1 Takara-machi, Kanazawa 920-0934, Japan

(Received February 23, 2007/Revised June 12, 2007/Accepted June 25, 2007/Online publication August 19, 2007)

Chronic infection with hepatitis B virus (HBV) is a major risk factor for hepatocellular carcinoma. The HBV X protein (HBx) is thought to have oncogenic potential, although the molecular mechanism remains obscure. Pathological roles of HBx in the carcinogenic process have been examined using rodent systems and no report is available on the oncogenic roles of HBx in human cells *in vitro*. We therefore examined the effect of HBx on immortalization and transformation in human primary cells. We found that HBx could overcome active RAS-induced senescence in human immortalized cells and that these cells could form colonies in soft agar and tumors in nude mice. HBx alone, however, could contribute to neither immortalization nor transformation of these cells. In a population doubling analysis, an N-terminal truncated mutant of HBx, HBx-D1 (amino acids 51–154), which harbors the coactivation domain, could overcome active RAS-induced cellular senescence, but these cells failed to exhibit colonigenic and tumorigenic abilities, probably due to the low expression level of the protein. By scanning a HBx expression library of the clustered-alanine substitution mutants, the N-terminal domain was found to be critical for overcoming active RAS-induced senescence by stabilizing full-length HBx. These results strongly suggest that HBx can contribute to carcinogenesis by overcoming active oncogene-induced senescence. (*Cancer Sci* 2007; 98: 1540–1548)

Chronic infection with HBV is a major risk factor for HCC worldwide. HBV belongs to the Hepadnavirus family. Its genome is a 3.2-kb, circular, partially double-stranded DNA molecule with four overlapping open reading frames: PC-C, PS-S, P and X.[1] The HBV genome, which is converted to covalently closed circular DNA in the nucleus after infection, serves as the template for transcription, generating the four viral transcripts that encode the HBV core and polymerase polypeptides, the large surface antigen polypeptide, the middle and major surface antigen polypeptides, and the HBx polypeptide. HBV replicates by reverse transcription of viral pregenomic 3.5-kb RNA using the HBV polymerase that catalyzes RNA-dependent DNA synthesis and DNA-dependent DNA synthesis.[1,2] It is converted into the 3.2-kb partially double-stranded genomic DNA inside the viral capsid.

The critical role of HBV chronic infection in HCC has been well established etiologically, whereas the mechanism by which HBV causes transformation of hepatocytes remains unclear.[3–5] HBx has long been suspected of playing a positive role in hepatocarcinogenesis, as avian hepadnaviruses missing the X open reading frame seem not to be associated with HCC. HBx consists of 154 aa and is a multifunctional regulator that modulates many host cell functions through its interactions with a variety of host factors.[5] HBx consists of both a negative regulatory domain[6] and a coactivation domain that is required for the augmentation of virus and host genes.[7,8] HBx was reported to transform rodent immortal cells *in vitro*,[9,10] and a high incidence of HCC has been reported in transgenic mice overexpressing HBx.[11,12] However, the functional role of HBx in the transformation is still controversial. Some independent groups proposed collaborating roles of HBx in the hepatocarcinogenic process.[13–15] Although these reports are informative, all were experimentally assessed in rodent systems. Because mouse and human primary cells have different telomere biology,[16] DNA damage check point control mechanisms and cell cycle progression,[17,18] developing a human system to address the functional role of HBx is critically important. Here we report that we established human fibroblast cells stably expressing HBx protein and analyzed the effects of HBx expression on the ability to confer an immortal phenotype and tumorigenic potential.

Materials and Methods

Retroviral vectors. All constructs for the expression of HBx (subtype adr) proteins, pNKF-HBx (aa 1–154), pNKF-HBx-D1 (aa 1–50) and pNKF-HBx-D5 (aa 51–154) have been described previously.[8] The retrovirus vectors pBabe-puro, hygro, puro-H-RAS^{V12} hygro-hTERT and pWZL-blast were kindly provided by W. C. Hahn (Dana-Farber Cancer Institute, Harvard).[19,20] To construct pBabe-blast, the blasticidin S cDNA of pWZL-blast was used as a template to amplify the PCR products of blasticidin S with the primer set of AAGCTTACCATGGCCAAGCCTTTGT and ATCGATTTAGCCCTCCCACACATAA, generating an artificial *Hind*III site at the 5-end and a *Cla*I site at the 3′-end, respectively. The HBx cDNA of pNKF-HBx was used as a template to amplify the PCR products of HBx with a primer set of TGATCAATGGACTACAAAGACGAT and CTCGAGAGAT-CTTTAATTAATTAA, generating an artificial *Fba*I site at the 5-end and an *Xho*I site at the 3′-end, respectively. The PCR products were digested and inserted into the *Bam*HI and *Sal*I sites of the pBabe-blast vector. The *Eco*RI and *Bgl*II fragments of HBx-D1 and HBx-D5 from pNKF-HBx-D1 and pNKF-HBx-D5 were, respectively, inserted into the *Eco*RI and *Bgl*II sites of the pBabe-blast-HBx vectors. An alanine scanning method was applied to construct a series of HBx clustered alanine substitution mutants (designated 'cm') by site-directed mutagenesis. The mutagenesis was carried out using a splicing PCR method with all of the mutated oligonucleotide primer sets. The target sequence of seven aa residues was changed to AAASAAA, and all of the HBx-encoding DNA fragments bearing the clustered mutations were introduced into the *Eco*RI and *Bam*HI sites of pNKFLAG, generating the pNKF-Xcm1 to pNKF-Xcm21 constructs. The

[3]To whom correspondence should be addressed.
E-mail: semuraka@kenroku.kanazawa-u.ac.jp

Abbreviations: aa, amino acid; DMEM, Dulbecco's modified Eagle's medium; HBV, hepatitis B virus; HBx, hepatitis B virus X protein; HCC, hepatocellular carcinoma; hTERT, human telomerase reverse transcriptase; OIS, oncogene-induced senescence; PCR, polymerase chain reaction; PD, population doubling; SA-β-gal, senescence-associated β-galactosidase; SDS-PAGE, sodium dodecylsulfate-polyacrylamide gel electrophoresis.

doi: 10.1111/j.1349-7006.2007.00579.x

*Eco*RI and *Bgl*II fragments of HBx-cm1 to HBx-cm21 from pNKF-Xcm1 to pNKF-Xcm21 were, respectively, inserted into the *Eco*RI and *Bgl*II sites of the pBabe-blast-HBx vectors. All of the constructs were sequenced by the dideoxy method using the *Taq* sequencing primer kit and a DNA sequencer (370A; Applied Biosystems).

Virus production and cell lines. Amphotropic retroviruses were produced by transfection of the 293T producer cell line with a retroviral vector and a vector encoding replication-defective helper viruses, pCL-Ampho (Imgenex), using FuGENE 6 transfection reagent (Roche Applied Science) according to the manufacturer's recommendations. Two days after the transfection, culture supernatants were collected, filtered, supplemented with 4 μg/mL polybrene, and used for infection. Two days after the infection, drug selection of infected cells was started, and the selected populations were used in all of the experiments. Infected cell populations were selected in puromycin (1.0 μg/mL), blasticidin S (4 μg/mL) and hygromycin (80 μg/mL) for up to 2 weeks.

Cell culture. Human lung fibroblasts (TIG3) from the Japanese Collection of Research Bioresources were maintained in DMEM with 10% heat-inactivated fetal bovine serum (JRH Biosciences). Human foreskin fibroblasts, BJ and BJ-hTERT-LT-ST-H-RAS^{V12} cells were maintained as described previously.[19] These human fibroblasts were not clonal and were maintained as populations. BJ cells and TIG3 cells have a finite lifespan, and were used at PD between 25 and 35. PD were determined using the formula:

$$PD = Log(Nf/Ni)/Log2,$$

where Nf = the number of cells counted and Ni = the number of cells seeded. Comparisons of means and standard deviations were carried out using the unpaired *t*-test.

Western blot analysis. Cells were harvested, washed with phosphate-buffered saline (–), and sonicated in a lysis buffer (50 mM Tris-HCl [pH 7.4], 200 mM NaCl, 1 mM ethylenediaminetetraacetic acid, 10% glycerol, 1 mM phenylmethylsulfonyl fluoride, 10 μg/mL leupeptin, 10 μg/mL aprotinin and 10 μg/mL dithiothreitol). Total lysates were fractionated by SDS-PAGE, transferred onto nitrocellulose membranes and subjected to western blot analysis with antibodies. Anti-FLAG M2 antibody and anti-β-actin antibody were from Sigma. Anti-RAS antibody F-235 (sc-29), anti-p53 antibody DO-1 (sc-126) and anti-p21 antibody F-5 (sc-6246) were from Santa Cruz. Anti-p16 antibody was from BD PharMingen. The proteins were visualized by enhanced chemiluminescence according to the manufacturer's instructions (Amersham).

Analysis of senescence. SA-β-Gal staining was carried out using the Senescence Detection Kit (Oncogene) as instructed by the manufacturer. For each sample, at least 200 cells were counted in randomly chosen fields.

Telomerase activity assays. Total lysates of cells were subjected to the telomerase repeat amplification protocol using a TRAPEZE kit (Intergen) according to the manufacturer's instructions.

Soft-agar colony formation assays. Soft-agar growth assays were carried out as described previously.[19] At the time of plating in soft agar, cultures were trypsinized and counted, and 5×10^3 or 5×10^4 total cells were mixed with 1.5 mL of 0.35% Noble agar-DMEM (top layer) and then poured on top of 5 mL of solidified 0.7% Noble agar-DMEM (bottom layer) in 6-cm-diameter dishes. After 3 weeks, colonies were counted, and pictures were taken.

Tumorigenicity assays. A total of 1×10^6 cells were resuspended in 50 μL Matrigel solution (BD Matrigel Basement Membrane Matrix HC; BD Biosciences) and immediately injected subcutaneously into 8-week-old female nude mice (BALB/cAnNCrl-nu BR). 2-D tumor sizes were measured once a week. The tumor volume (mm^3) was calculated using the formula (length × width^2)/2.[21]

Results

Effect of HBx on cellular senescence of human primary cells. During immortalization, human cells differ from rodent cells in the regulation of telomere length[22,23] and cell cycle checkpoints.[24,25] Human cells must bypass two barriers to become immortalized: replicative senescence and crisis. Replicative senescence is characterized by an irreversible growth arrest but continued metabolic activity.[26] Crisis is characterized by widespread cell death.[26,27] By the introduction of hTERT, human primary cells avoid these two barriers and can become immortalized.[28–30]

It is possible that HBx contributes to the immortalization process of human primary cells, but not to the cellular transformation process. If so, it may facilitate cellular transformation indirectly by overcoming two crises, M1 and M2. To study whether this does facilitate cellular transformation, it is best to use human primary hepatocytes as HBV is a hepatotropic virus. However, human primary hepatocytes are almost impossible to obtain for such an experimental approach. HBx exhibits its transactivation function not only in hepatoma cell lines but also in various carcinoma and sarcoma cell lines. Under these situations, we addressed whether HBx contributes to the immortalization of human primary fibroblasts, BJ cells and TIG3 cells that have been well studied for cellular senescence and immortalization. We used hTERT-introduced BJ and TIG3 cells for positive controls of immortal cells.

The human primary fibroblasts, BJ cells and TIG3 cells were infected with the HBx-expression retroviruses and cultured in the presence of the selection drug, blasticidin S. The drug-resistant polyclonal cells were selected and characterized. Three different constructs of HBx were used to map the responsible domain: full-length HBx (HBx-wt), HBx-D1, which lacks the N-terminal negative regulatory domain, and HBx-D5, which lacks the coactivation domain (Fig. 1a). First we examined HBx expression in the primary human fibroblasts. We found that full-length HBx and HBx-D5 were highly but equally expressed, whereas expression of HBx-D1 was very weak in the blasticidin S-selected clones (Fig. 1b). We hypothesized that HBx expression may confer an immortal phenotype, which could contribute to cellular transformation and tumorigenesis, but we observed that the BJ cells expressing HBx proteins stopped dividing at PD 69.6 ± 0.9 (errors ± SD) (HBx-wt), PD 66.6 ± 1.6 (HBx-D5), PD 66.1 ± 1.4 (HBx-D1) and PD 60.5 ± 0.6 (control cells) (Fig. 1c). TIG3 cells, another human fibroblast, expressing HBx proteins stopped dividing at PD 77.2 ± 1.1 (HBx-wt), PD 75.1 ± 0.8 (HBx-D5), PD 75.1 ± 0.1 (HBx-D1) and PD 75.4 ± 0.2 (control cells) (Fig. 1d). Although a very minor extended lifespan (2–4 PD) was observed with HBx-wt-expressing primary human fibroblasts, the HBx protein could not elicit immortalization. We examined whether the effect of HBx on delay of cellular senescence was correlated with putative augmentation of telomerase activity in HBx-introduced BJ and TIG3 cells (Fig. 1e) as activation of the hTERT promoter was observed in hepatoma cell lines that were transiently cotransfected with the HBx expression vector and luciferase reporter vector of the hTERT promoter (S. Murakami *et al.* unpublished data, 2005). Telomerase activity in the extracts of cells expressing HBx-wt or HBx-D1 was slightly higher than that of cells expressing empty vector or HBx-D5 in both kinds of cells (Fig. 1e), but we failed to detect an increase in hTERT protein expression (data not shown). Therefore, the relevance of the weak augmentation of telomerase activity in the HBx-expressing primary cells remains unclear.

Effect of HBx on immortalized BJ-hTERT cells. Next, we addressed whether HBx facilitates the cellular transformation process

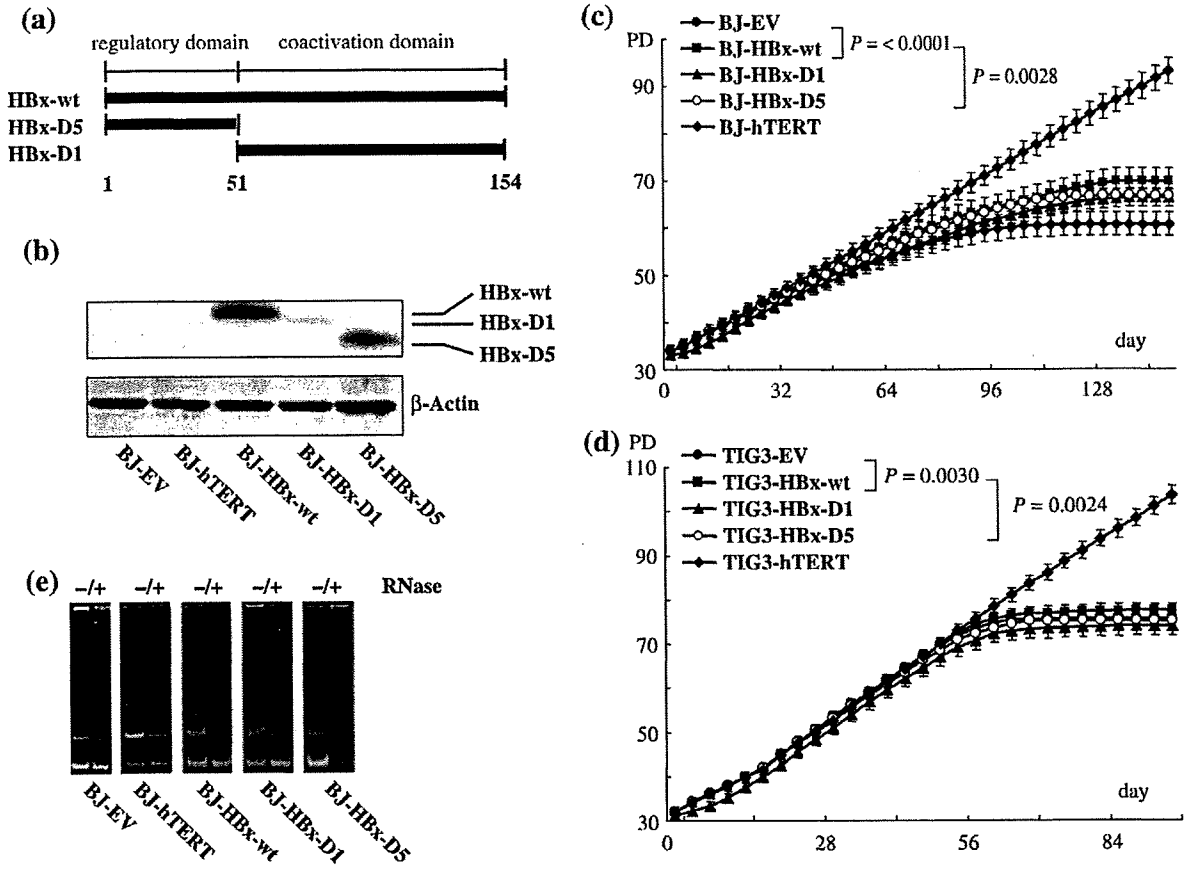

Fig. 1. Hepatitis B virus protein X (HBx) can not immortalize human primary cells, but weakly affects cellular senescence and telomerase activity. (a) Schematic representation of the HBx proteins.[5,8] The amino acids (aa) of full-length HBx (154 aa residues) and truncated HBx are shown. HBxD1 harbors the carboxy-terminal coactivation domain, spanning aa residues 51–154, whereas, HBxD5 harbors the amino-terminal negative regulatory domain, spanning aa residues 1–50. (b) Expression of HBx, HBx-D1 and HBx-D5 proteins in infected BJ cells. Total cell lysates of BJ cells infected with the empty vector (EV), human telomerase reverse transcriptase (hTERT), HBx, HBx-D1 and HBx-D5 expression retroviruses were fractionated by sodium dodecylsulfate–polyacrylamide gel electrophoresis and subjected to western blot analysis with anti-FLAG M2 antibody. (c) Effect of HBx on replicative senescence in BJ cells. BJ cells were infected with a control vector (filled circles) or hTERT (filled diamonds) and with a retrovirus encoding wild-type HBx (filled squares), HBx-D1 (filled triangles) or HBx-D5 (open circles). Cells infected with pBabe-puro- and pBabe-blast were selected with 1 μg/mL puromycin and 4 μg/mL blasticidin S, respectively. After 8 days of drug selection, triplicate samples of 1×10^5 cells were plated and grown under normal conditions (day 0). (d) Effect of HBx mutants on replicative senescence in TIG3 cells. Symbols are the same as in (c). (e) Telomerase activity in BJ cells as demonstrated by telomerase activity assay (TRAP). Total cell lysates (200 ng) prepared from BJ cells infected with control vector, hTERT, HBx, HBx-D1, and HBx-D5 were subjected to TRAP assay using a TRAPEZE kit (Intergen).

using human immortal cells. For this purpose, we used BJ-hTERT cells – these were BJ-derived cells immortalized by the introduction of hTERT, as characterized previously.[19] HBx-wt as well as its truncated mutants had no effect on cell proliferation, telomerase activity or cell transformation. Using the newly established TIG3-hTERT cells, we confirmed that the stable expression of HBx, XD1 or XD5 did not affect cell proliferation or cell transformation (data not shown). These results indicate the inability of HBx alone to transform these human immortalized cells.

Ability of HBx to overcome H-RAS^{V12}-induced senescence in BJ cells immortalized by hTERT Seeing as HBx did not exhibit the ability to immortalize primary human fibroblasts or to elicit transformation into hTERT-induced immortal primary human fibroblasts, we considered whether HBx functioned together with an oncogene and induced cell transformation. Senescence induced by active oncogene expression (OIS), such as oncogenic RAS, is one of the anticancer processes in which tumor suppressors and their related networks are involved, as demonstrated *in vitro* and recently also *in vivo*.[31,32] Overcoming OIS is critical for cellular transformation *in vitro* and cancerous cell proliferation *in vivo*.[31] Therefore, we addressed whether HBx has a collaborating role in transforming cells in the presence of oncogenic RAS or in overcoming RAS-induced senescence.

To examine the effect of HBx on RAS-induced senescence-like growth arrest, we introduced H-RAS^{V12} into BJ-hTERT, BJ-hTERT-HBx-wt, BJ-hTERT-HBx-D1 and BJ-hTERT-HBx-D5 cells using a retrovirus (Fig. 2d). BJ-hTERT cells expressing H-RAS^{V12} stopped proliferating within several days of RAS introduction. In contrast, BJ-hTERT cells expressing both H-RAS^{V12} and HBx-wt (BJ-hTERT + H-RAS^{V12} + HBx-wt) continued to proliferate to more than 80 PD (Fig. 2a). Although HBx-D1 also demonstrated the ability to overcome active RAS-induced senescence, HBx-D5 failed to overcome OIS (Fig. 2a). We also found that the growth rate of BJ-hTERT + H-RAS^{V12} + HBx-wt cells was much higher than that of BJ-hTERT + H-RAS^{V12} + HBx-D1 cells, probably reflecting the fact that some portion of the latter cells were positive for SA-β-gal (Fig. 2b,c). Consistent with this result, cells staining positive for SA-β-gal were significantly fewer in BJ-hTERT +

doi: 10.1111/j.1349-7006.2007.00579.x

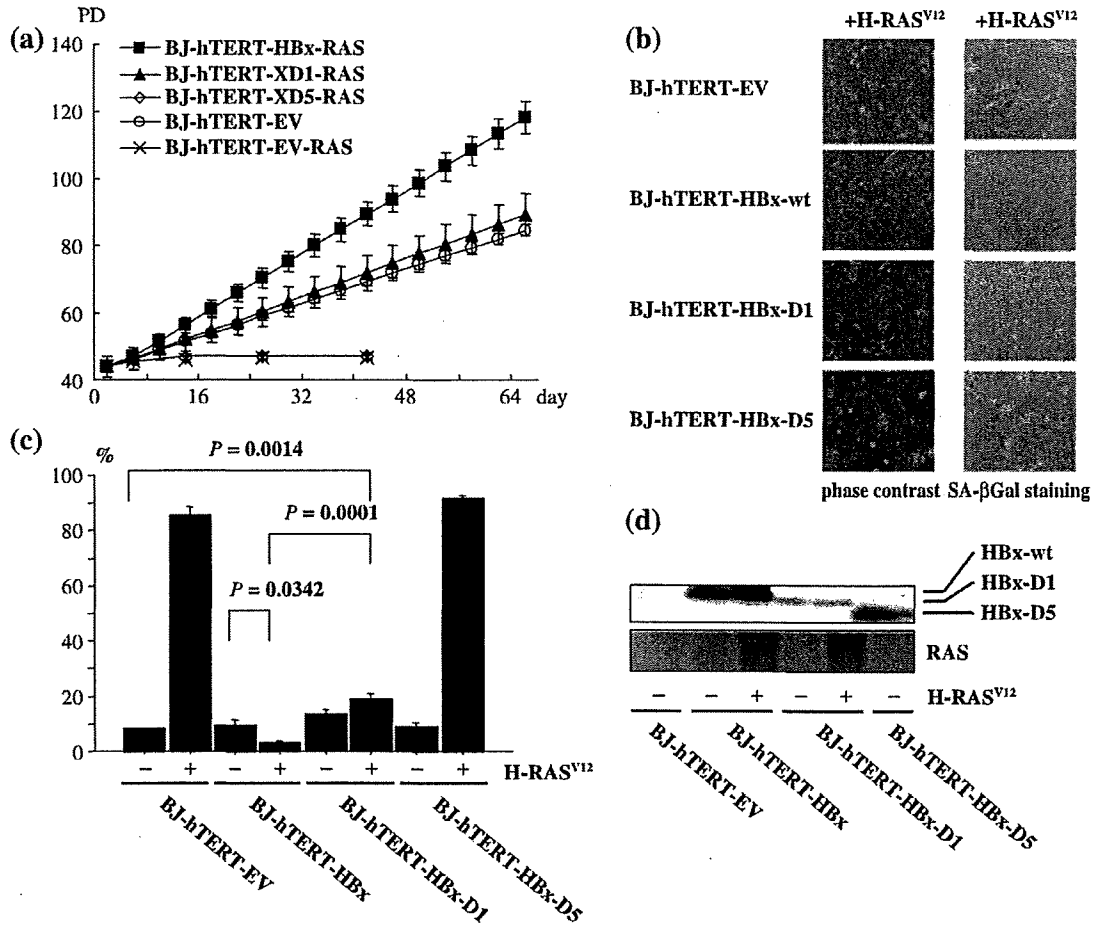

Fig. 2. Hepatitis B virus protein X (HBx) can overcome H-RAS^{V12}-induced cellular senescence of human immortalized cells. (a) Effect of HBx on H-RAS^{V12} induced senescence. BJ-human telomerase reverse transcriptase (hTERT) cells (open circles) and H-RAS^{V12}-induced BJ-hTERT-HBx-wt (filled squares), BJ-hTERT-HBx-D1 (filled triangles), BJ-hTERT-HBx-D5 (filled diamonds) cells and BJ-hTERT-empty vector (EV) (cross) are shown. After 10 days of drug selection at population doubling (PD) 42, triplicate samples of 1×10^5 cells were plated and grown under normal conditions (day 0). (b) HBx overcomes H-RAS^{V12}-induced senescence of human immortalized cells. H-RAS^{V12} and EV, full-length or truncated forms of HBx were introduced into BJ-hTERT cells. Left panel shows photographs 10 days after infection of the H-RAS^{V12}-expression retrovirus. Right panels show senescence-associated β-galactosidase (SA-β-Gal) staining 10 days after infection. (c) The percentage of cells positive for SA-β-Gal was determined in BJ cells stably expressing HBx-wt, HBx-D1, HBx-D5 or empty vector, with or without H-RAS^{V12} on day 9 after infection. Bars = mean ± SD. (d) Western blot analysis of RAS-induced cells. Total cell lysates from BJ-hTERT cells stably expressing HBx-wt, HBx-D1, HBx-D5 or EV together with or without H-RAS^{V12} were prepared and fractionated by sodium dodecylsulfate-polyacrylamide gel electrophoresis, then subjected to western blot analysis. HBx-wt, HBx-D1 and HBx-D5 were detected with anti-FLAG M2 antibody. RAS protein was detected with anti-RAS antibody.

H-RAS^{V12} + HBx-wt than in BJ-hTERT + H-RAS^{V12} + HBx-D1 (Fig. 2c). These results indicate that HBx-wt has the ability to overcome RAS-induced senescence. HBx-D1, the coactivator domain of HBx, seems to be indispensable and sufficient for overcoming RAS-induced senescence analyzed by the PD analysis, although HBx-D1 did not show the same ability as HBx-wt. The incomplete ability of HBx-D1 may be due to the low expression of HBx-D1 in the blastcidin S-selected clones in BJ-hTERT cells, as observed with the BJ cells (see Discussion).

HBx protein is required for anchorage-independent growth and tumor formation in nude mouse in response to H-RAS^{V12}. HBx can overcome RAS-induced senescence (examined by the PD analysis) and can indicate that HBx and RAS can induce cell transformation. Therefore, we examined whether BJ-hTERT + H-RAS^{V12} + HBx-wt and BJ-hTERT + H-RAS^{V12} + HBx-D1 cells can form colonies in soft agar. We found that BJ-hTERT + H-RAS^{V12} + HBx-wt cells showed cell number-dependent formation of colonies, which were much smaller size than those of control cells, BJ-hTERT + H-RAS^{V12} + SV40 LT + ST$^{(20,33)}$ (Fig. 3a,b). In contrast, BJ-hTERT + H-RAS^{V12} + HBx-D1 cells could not form colonies in soft agar (Fig. 3a), although these cells overcame RAS-induced senescence. This result strongly suggests that HBx-D1 is not equivalent to HBx-wt in its ability to make colonies in soft agar.

Next we tested the tumor-forming ability of BJ-hTERT + H-RAS^{V12} + HBx-wt or HBx-D1 cells in nude mice. BJ-hTERT + H-RAS^{V12} + HBx-wt cells were found to form tumors in four of eight mice, although these tumors grew much more slowly and were much smaller than those formed by BJ-hTERT + H-RAS^{V12} + SV40 LT + ST cells (eight of eight animals) (Fig. 3c). In contrast, BJ-hTERT + H-RAS^{V12} + HBx-D1 cells did not generate tumors in nude mice (Fig. 3c), consistent with the results of the soft-agar assay. These results indicate that HBx contributes to cellular transformation by collaborating with active RAS in human immortalized cells. To our knowledge, this is the first report showing that HBx plays a critical role in

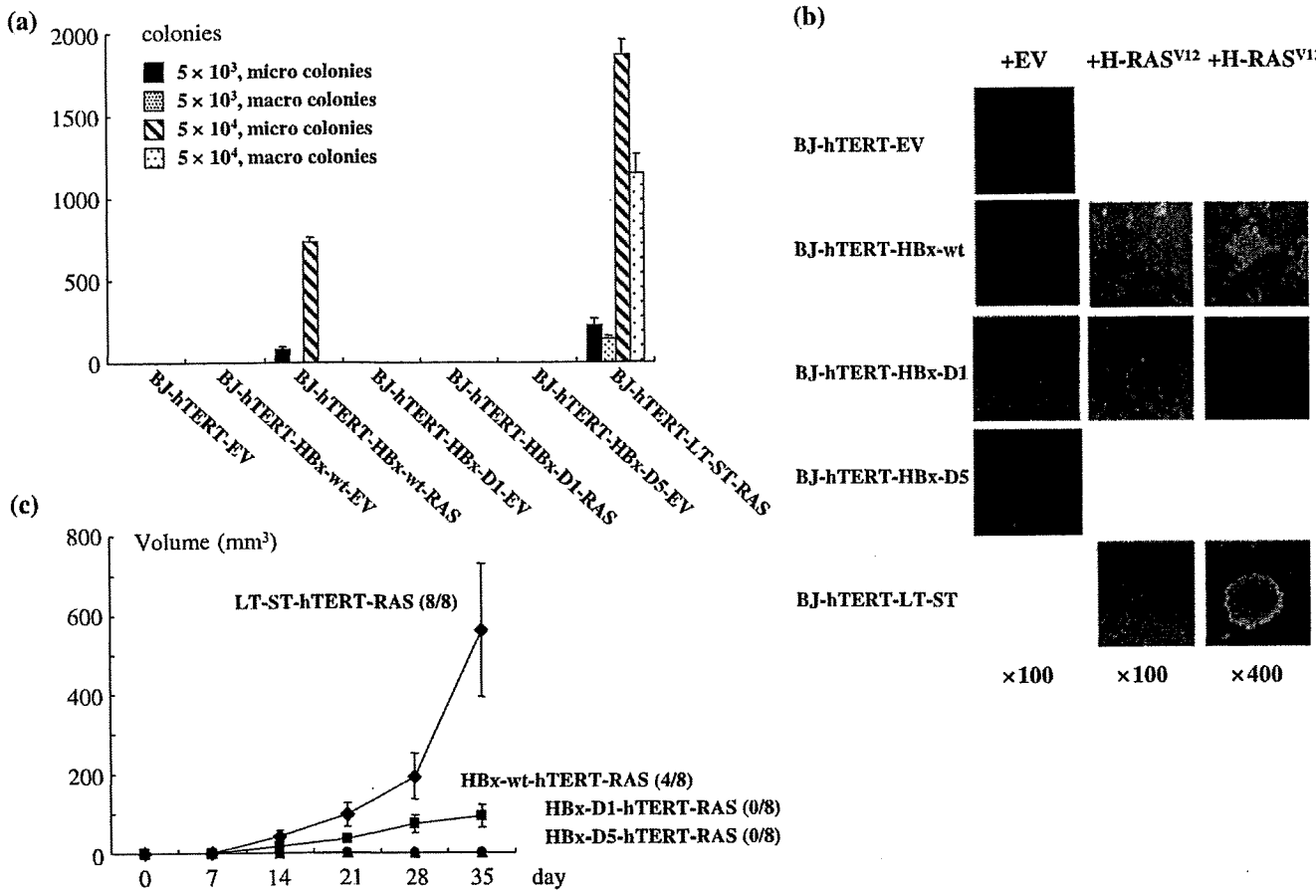

Fig. 3 (a,b) Anchorage-independent growth in soft agar and (c) tumorigenicity and tumor-forming ability in nude mice of cells expressing hepatitis B virus X protein (HBx) and H-RAS^{V12}. (a) Soft-agar assays were carried out as described in Materials and Methods.[19] After 3 weeks, colonies were counted and pictures were taken. The colony-forming ability of BJ-human telomerase reverse transcriptase (hTERT) cells stably expressing wild-type or truncated HBx with or without H-RAS^{V12} is indicated at the bottom. H-RAS^{V12}-introduced BJ-hTERT-LT-ST cells were the positive control. (b) Morphology of colonies in the soft-agar assay. Colonies were photographed 21 days after seeding. (c) Tumor formation in nude mice was carried out as described previously in Materials and Methods.[19,21] Tumor sizes were measured once a week. Each point on the graph represents the average volume of tumors. BJ-hTERT-LT-ST-RAS (filled diamonds), BJ-hTERT-HBx-RAS (filled squares), BJ-hTERT-HBx-D1 (filled circles), and BJ-hTERT (filled triangles) cells are shown. Error bars indicate the mean ± SD for each time point.

cellular transformation, collaborating with active RAS in human immortalized cells.

Effects of HBx on p16 and p21 expression and the ability of HBx to overcome RAS-induced senescence. Overexpression of RAS causes oncogene-induced premature senescence in normal human fibroblasts (Fig. 4c) and hTERT-immortalized human fibroblasts (Fig. 2a), but RAS failed to induce premature senescence in HBx-wt- or HBx-D1-introduced BJ-hTERT cells (Fig. 2a). We next examined the effect of stable expression of HBx in BJ cells with or without expression of hTERT, as interference with both the p53 and pRb pathways is necessary to avoid RAS-induced cellular senescence, in which p16 and p21 are the critical downstream effectors of pRb and p53, respectively. Expression of p16 and p21 was upregulated in HBx-wt- or HBx-D1-introduced BJ-hTERT cells; however, HBx-D5 has no ability to induce the expression of these genes. The presence of H-RAS^{V12} resulted in downregulation of the augmented expression of p16 and p21 in HBx-wt- or HBx-D1-introduced BJ cells and BJ-hTERT cells (Fig. 4a,b). These results suggest that HBx can suppress expression of p53, p16 and p21 in H-RAS^{V12}-introduced cells, contributing to overcoming RAS-induced senescence. Next we examined whether HBx-wt and H-RAS^{V12} not immortalized by hTERT were sufficient for cellular transformation. We introduced H-RAS^{V12} into BJ-HBx-wt, BJ-HBx-D1 and BJ-HBx-D5 cells and analyzed them by PD analysis and soft-agar colony assay. In the PD analysis, H-RAS^{V12}-introduced BJ-HBx-wt and BJ-HBx-D1 cells did overcome RAS-induced cellular senescence but stopped cell division at PD 62, which is approximately the cellular senescence of BJ cells (Figs 1c,4c), whereas H-RAS^{V12}-introduced BJ-HBx-D5 did not overcome senescence and stopped cell division. These results suggest that HBx can overcome RAS-induced senescence but can not immortalize the cells (Fig. 4c). In the soft-agar colony formation assay, BJ-HBx-wt-H-RAS^{V12} and BJ-HBx-D1-H-RAS^{V12} could but BJ-HBx-D5-H-RAS^{V12} could not form very tiny colonies, suggesting that HBx-wt and H-RAS^{V12} in the absence of hTERT may enable the cells to proliferate in an anchorage-independent manner (data not shown).

As HBx-D1, which was very weakly expressed, exhibited almost the same ability as HBx-wt to upregulate the tumor suppressor genes and to overcome RAS-induced senescence in these cells, we wondered whether HBx-D1 missing the N-terminal domain may have some negative effect on cell proliferation. Because the transient expression level of HBx-D1 in BJ cells was similar to those in HepG2 cells, as reported previously

doi: 10.1111/j.1349-7006.2007.00579.x

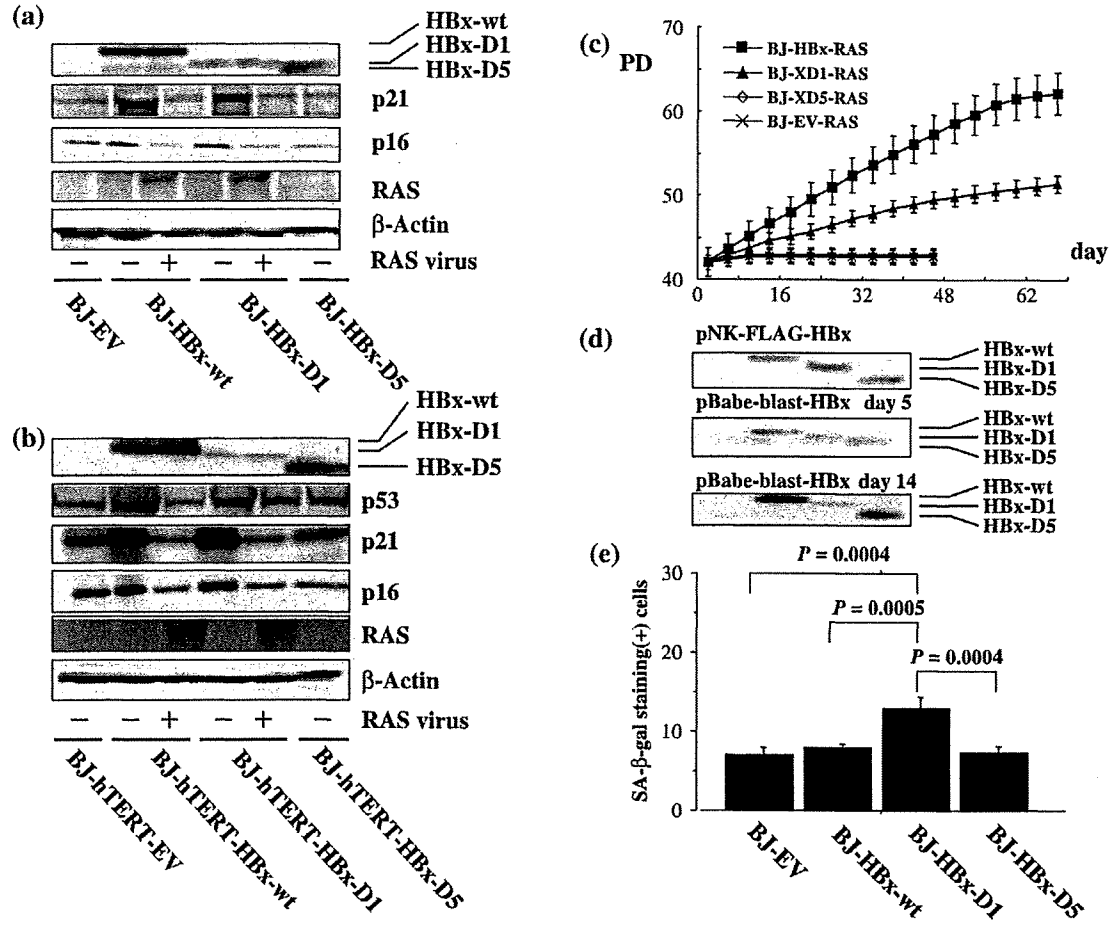

Fig. 4. Effect of hepatitis B virus X protein (HBx) on p16 and p21 expression and the ability of HBx to overcome H-RAS^{V12}-induced cellular senescence of human normal cells. Total cell lysates from BJ-human telomerase reverse transcriptase (hTERT) cells stably expressing HBx-wt, HBx-D1, HBx-D5 or empty vector together with or without H-RAS^{V12} were prepared, and fractionated by sodium dodecylsulfate–polyacrylamide gel electrophoresis (SDS-PAGE), then subjected to western blot analysis. Expression of (a) p16 and p21 proteins and (b) p53, p16 and p21 proteins. (c) Effect of HBx on H-RAS^{V12}-induced senescence. Population doublings (PD) of H-RAS^{V12}-induced BJ-HBx-wt (filled squares), BJ-HBx-D1 (filled triangles), BJ-HBx-D5 (open diamonds) and BJ-EV (cross) cells are shown. After 10 days of drug selection, at PD 44, triplicate samples of 1×10^5 cells were plated and grown under normal conditions (day 0). (d) Expression of HBx, HBx-D1 and HBx-D5 proteins in infected BJ cells. Total cell lysates of BJ cells transfected with mammalian expression plasmids of FLAG-HBx-wt, FLAG-HBx-D1 and FLAG-HBx-D5 were fractionated by SDS-PAGE and subjected to western blot analysis with anti-FLAG M2 antibody (upper panel). Total cell lysates of BJ cells infected with the empty vector (EV), HBx-wt, HBx-D1 and HBx-D5 expression retroviruses were fractionated by SDS-PAGE and subjected to western blot analysis with anti-FLAG M2 antibody (middle and bottom panel). (e) The percentage of cells positive for senescence-associated β-galactosidase (SA-β-Gal) was determined in BJ cells stably expressing HBx-wt, HBx-D1, HBx-D5 or empty vector (EV) on day 40 after infection. Bars = mean ± SD.

(Fig. 4d),[8] it was not due to the construct design of the vector. The expression of HBx-D1 was slightly lower than those of HBx-wt and HBx-D5 on day 5 after selection, much lower on day 10 after selection (data not shown). On day 14 after selection, the expression of HBx-D1 reached the lowest level, and after day 14 that expression level was kept (Figs 1b,4d). HBx-D1-introduced BJ cells grew slower than HBx-wt- or HBx-D5-introduced BJ cells (data not shown) and contained more SA-β-Gal-positive cells during proliferation (Fig. 4e). These results suggest that cells expressing lower levels of HBx-D1 proliferated more than cells expressing higher levels of HBx-D1, due to some toxic or antiproliferative effect of the coactivation domain of HBx in the human primary cells (see Discussion).

Important region of HBx for overcoming cellular senescence and anchorage-independent growth. As HBx exhibited the ability to overcome active RAS-induced senescence, we next tried to identify the critical regions of HBx for overcoming cellular senescence. BJ-hTERT cells were infected with retroviruses expressing one of the clustered alanine-substituted mutants covering all parts of HBx,[34] and a series of cell clones stably expressing these HBx-cm mutants, BJ-hTERT-HBx-cm, was established (Fig. 5). H-RAS^{V12} was then introduced into BJ-hTERT-HBx-cm1 to BJ-hTERT-HBx-cm21 cells and cell proliferation was examined. The regions covering HBx-cm8 to HBx-cm10, and those covering HBx-cm19 to HBx-cm21 were found to be not critical for overcoming active RAS-induced senescence and anchorage-independent growth as the BJ-hTERT-RAS clones expressing these HBx-cm mutants proliferated and formed colonies in soft agar, similar to BJ-hTERT-HBx-wt-H-RAS^{V12} cells. The BJ-hTERT-RAS clones expressing HBx-cm1 to HBx-cm7, and those expressing HBx-cm14 to HBx-cm16, were like BJ-hTERT-HBx-D1-RAS, which can grow but at a much reduced rate compared with BJ-hTERT-HBx-RAS cells. The HBx regions covering HBx-cm11 to HBx-cm13, HBx-cm17

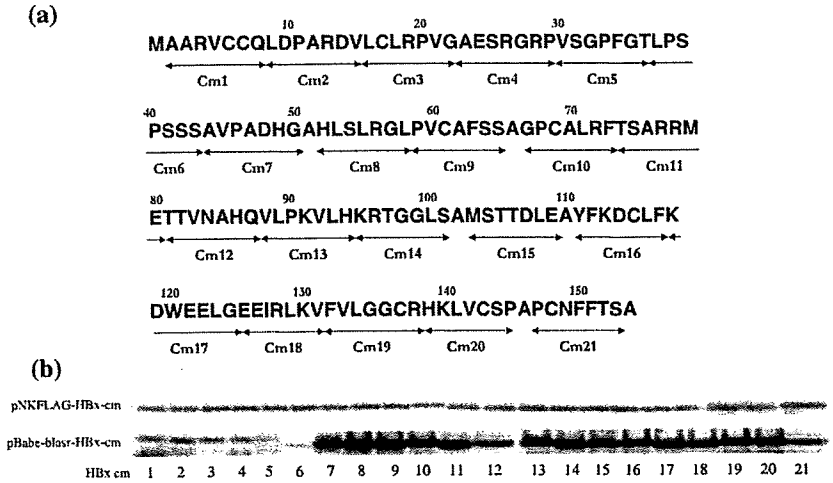

Fig. 5. Expression of hepatitis B virus X protein (HBx) library of clustered alanine substitution mutants in BJ-human telomerase reverse transcriptase (hTERT) cells. (a) Schematic representations of a series of clustered alanine substitution mutants (cm1 to cm21) of HBx. The amino acid locations of the clustered mutations are shown. (b) Detection of the mutated HBx proteins. Total cell lysates prepared from BJ-hTERT cells transfected with the mutant HBx expression vectors were fractionated by sodium dodecylsulfate–polyacrylamide gel electrophoresis and subjected to western blot analysis with anti-FLAG M2 antibody.

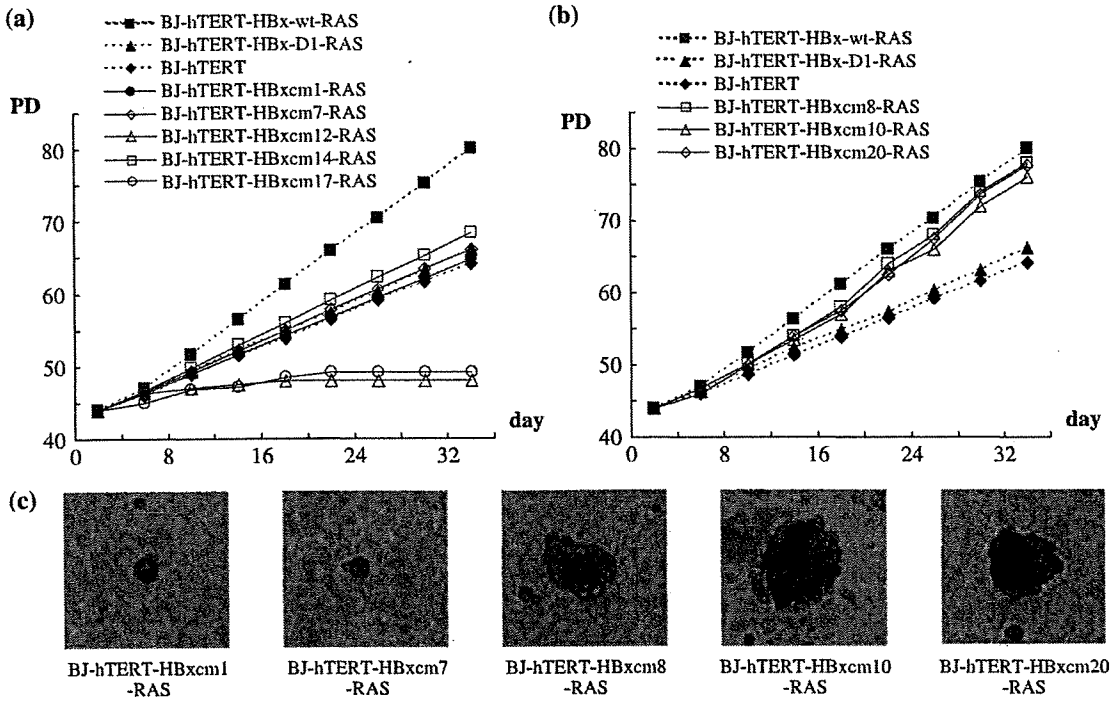

Fig. 6. Critical regions of hepatitis B virus X protein (HBx)-wt for tumorigenic function. (a) Effect of HBx-cm1–7 and HBx-cm11–18 failed to overcome H-RAS^{V12}-induced cellular senescence. Cell proliferation curves of several HBx-cm clones introduced with BJ-human telomerase reverse transcriptase (hTERT)-H-RAS$^{V(12)}$ in addition to those of BJ-hTERT cells (filled diamonds), H-RAS^{V12}-introduced BJ-hTERT-HBx-wt cells (filled squares) and BJ-hTERT-HBx-D1 cells (filled triangles) are shown. HBx-cm1, -cm7, -cm12, -cm14 and -cm17 were selected. HBx-cm1 (closed circles) and HBx-cm7 (open diamonds) represent HBx-cm1–7-introduced BJ-hTERT-H-RAS^{V12} cells. HBx-cm12 (open triangles) represents HBx-cm11–13-introduced BJ-hTERT-H-RAS^{V12} cells. HBx-cm14 (open squares) represents HBx-cm14–16-introduced BJ-hTERT-H-RAS^{V12} cells. HBx-cm17 (open circles) represents HBx-cm17 and HBx-cm18-introduced BJ-hTERT-H-RAS^{V12} cells. pBabe-puro-RAS-infected cells were selected with 1 μg/mL puromycin. After 10 days of drug selection at population doubling (PD) 44, triplicate samples of 1×10^5 cells were plated and grown under normal conditions. (b) Effect of HBx-cm8–10 and HBx-cm19–21 overcomes H-RAS^{V12}-induced cellular senescence. Cell proliferation curves of several HBx-cm clones introduced into BJ-hTERT-H-RAS^{V12} in addition to those of BJ-hTERT cells (filled diamonds), H-RAS^{V12}-introduced BJ-hTERT-HBx-wt cells (filled square) and BJ-hTERT-HBx-D1 cells (filled triangles) are shown. HBx-cm8 (open squares) and HBx-cm10 (open triangles) represent HBx-cm8–10-introduced BJ-hTERT-H-RAS^{V12} cells. HBx-cm20 (open diamonds) represents HBx-cm19–21-introduced BJ-hTERT-H-RAS^{V12} cells.

and HBx-cm18 were found to be critical for overcoming active RAS-induced senescence as the BJ-hTERT-RAS clones expressing these HBx-cm mutants failed to proliferate, meaning that these had no ability to overcome active RAS-induced cellular senescence at all (Fig. 6) (Table 1). Among the BJ-hTERT-HBx-cm cells, expression levels of HBx-cm1 to HBx-cm6 were very weak, like that of HBx-D1. Furthermore, the protein bands of HBx-cm1 to HBx-cm5 migrated slightly slower than those of HBx-cm6 and the other HBx-cm mutants in the coactivation domain in SDS-PAGE analysis (see Discussion).

doi: 10.1111/j.1349-7006.2007.00579.x

Table 1. Degree of proliferation of H-RAS^{V12}-introduced BJ-hTERT-HBx-cm cells

Cell type	Degree of proliferation
HBx-cm1†	+‡
HBx-cm2	+
HBx-cm3	+
HBx-cm4	+
HBx-cm5	+
HBx-cm6	+
HBx-cm7	+
HBx-cm8	++§
HBx-cm9	++
HBx-cm10	++
HBx-cm11	–
HBx-cm12	–¶
HBx-cm13	–
HBx-cm14	+
HBx-cm15	+
HBx-cm16	+
HBx-cm17	–
HBx-cm18	–
HBx-cm19	++
HBx-cm20	++
HBx-cm21	++

†HBx-cm1–21 in this table represent HBx-cm1–21-introduced BJ-hTERT-H-RAS^{V12} cells. ‡Same as BJ-hTERT-HBx-D1-H-RAS^{V12} cells. §Same as BJ-hTERT-HBx-wt-H-RAS^{V12} cells. ¶Senescence.

Discussion

Hepatitis B virus X protein has long been suspected to be positively involved in HBV-associated HCC, but its molecular role in hepatocarcinogenesis remains unclear. Although HBx is involved directly in the transformation of immortal rodent cells *in vitro* and in tumor formation in the livers of nude mice, the oncogenic activity of HBx itself remains to be elicited as the reproducibility of these experiments has been seriously controversial.[5] Furthermore, the positive role of HBx has not been addressed with human primary cells or human immortal cells. To our knowledge, our report is the first to show that HBx retains the ability to overcome RAS-induced senescence of immortalized human cells, although it is not sufficient for immortalizing human primary cells or transforming human immortal cells. hTERT-immortalized human cells stably expressing HBx-wt and RAS can form colonies in soft agar and tumors in nude mice in a cell-number-dependent manner. HBx can overcome RAS-induced senescence of BJ cells, but HBx-wt and active RAS could not immortalize the human fibroblasts. Although our findings are different to a report showing that HBx itself retains the transforming ability in NIH3T3 cells,[9] they are similar to results in rodent immortal embryonic fibroblast cells.[10]

To determine the region of HBx responsible for the ability to overcome RAS-induced senescence, we used two truncation mutants: HBx-D1 (aa 51–154), which exhibits transcriptional coactivation function and augments HBV transcription and replication,[8] and HBx-D5 (aa 1–50), which harbors the negative regulatory domain of transcriptional modulation.[6] When HBx-D1 and H-RAS^{V12} were introduced into BJ-hTERT cells, HBx-D1 was similar to wild-type HBx in overcoming RAS-induced senescence in the PD analysis and in SA-β-gal staining. Therefore, HBx-D1 alone seems to be sufficient for overcoming active RAS-induced senescence and for anchorage-independent growth, but it is not sufficient for BJ-hTERT + H-RAS^{V12} + HBx-D1 cells to form visible colonies in soft agar and tumors in nude mice. HBx alone may be sufficient for overcoming RAS-induced senescence, but hTERT is required for immortal proliferation of the transformed cells with H-RAS^{V12} and HBx. As HBx-D1 exhibits a similar ability to HBx-wt in overcoming RAS-induced senescence and anchorage-independent growth, but not in immortalizing human fibroblasts, HBx-D1 may harbor all of the critical abilities of HBx. However, HBx-D1 is different from HBx-wt in the ability to form visible colonies in soft agar and to form tumors in nude mice.

The coactivation function was recently mapped by scanning a HBx library of clustered alanine substitution mutants (HBx-cm library), and two separate sequences in HBx-D1 were found to be critical.[8] Using the same HBx-cm library, we attempted to map the sequences critical for overcoming RAS-induced senescence. We have identified three different phenotypes among the HBx-cm mutants: those phenotypes are like HBx-wt, HBx-D1 and HBx-D5 (Fig. 6). HBx-cm mutations within the D5 region, cm1 to cm7, have the ability to partially overcome OIS, whereas those within the D1 region (cm8–10, cm14–16 and cm 19–21) fail to exhibit the overcoming ability. The HBx-D5 phenotype is even found among the HBx-cm mutants (cm13, cm17 and cm18) that are defective in the coactivation function.[8] These results indicate that the ability to fully overcome OIS requires two putative functions carried by the D1 and D5 regions of the HBx protein. Because HBx-D5 does not have a positive or negative effect on RAS-induced senescence (Figs 2,3,4c), the negative regulatory domain may be active only in full-length HBx. The very low expression of HBx-D1 in human primary cells and hTERT-immortalized cells may be due to the selection result of clones, reflecting that a high level of HBx-D1 protein was eliminated due to a toxic effect of the coactivation domain,[5] or due to deletion of the N-terminal domain that has some critical role in stabilizing HBx in the expression system. Both of these may actually occur. The former is supported by the enrichment of cells expressing HBx-D1 during the early stages of drug selection. The latter is highly possible as expression levels of HBx-cm1 to HBx-cm6 covering most of the N-terminal domain were very low, as for HBx-D1. Pang *et al.* recently reported a stabilization mechanism of HBx through direct interaction with Pin1,[35] which binds phosphorylated serine and the next proline. The target serine residue is within the N-terminal domain or within the region covered by HBx-cm6. Interestingly, the HBx-cm1 to HBx-cm5 bands migrated more slowly than the HBx-cm6 band (Fig. 5b), supporting the possibility that the N-terminal domain may be critical for Pin1 binding to stabilize HBx. One interesting possibility that remains to be tested is that activation of the degradation pathway of HBx causes the toxic effect on cell proliferation. This possibility may explain the low expression of HBx-D1 and the cm mutants in the N-terminal domain. In this context, it remains unclear at present the reason for the rather stable expression of two bands of HBx-cm7 that seem to confer the same phenotype as HBx-D1 in the characterization of the cells.

The region of D1 that is responsible for overcoming RAS-induced senescence should be defined. Because some HBx-cm mutants defective in coactivation function still exhibit the ability to overcome OIS, it seems that the coactivation function is dispensable for the role. More than a dozen host factors have been reported to interact directly with the HBx-D1 region, including p53,[36,37] Smad4,[38] DDB1,[39,40] and two core subunits of the proteasome.[5] It is especially important to determine whether the binding of HBx to p53 is responsible for the ability to overcome RAS-induced senescence, as the direct binding of p53 to HBx was found to suppress p53-dependent gene activation.[5,37]

Although we have shown here that the D5 region of HBx has an indispensable biological role in anchorage-independent cell growth, the critical role of the D5 region in overcoming OIS remains obscure. The ability of the D5 region in full-length HBx